The Utility and Application of Non-Invasive Fluorescent Imaging in Murine Models of Allergic Asthma

by

Matthew S. Lytwyn

A Thesis submitted to the Faculty of Graduate Studies of
The University of Manitoba
in partial fulfilments of the

MASTER OF SCIENCE

Degree

Department of Physiology and Pathophysiology
University of Manitoba
Winnipeg, Manitoba, Canada

"…the definition between an entrepreneur and an employee is an employee goes to the cliff and looks over the cliff and says is there a balloon down there to catch me? Will I be safe? What happens if it hurts? What if I land on my neck? The entrepreneur, they said we need you to jump off a cliff, backs up ten feet to get a fucking run!"

-Todd McFarlane
Image Revolution (2014), Respect Films, United States

ACKNOWLEDGEMENTS

All I want to acknowledge is one thing from the entire process of completing this thesis; ***that it is finally over.*** I want to acknowledge this chapter of my life, regardless of who did and said what. Regardless of how long it took. Regardless of the responsibilities, both fulfilled and failed, of the individuals and institutions involved. Regardless of the pain, broken spirits, and losses and gains involved. That it is finally over...

…And I couldn't be happier…

….I also need a drink!

This thesis is dedicated to all the mice that gave their lives in to complete this degree.

They are the ***true*** scientists of this world.

1. TABLE OF CONTENTS

2. List of Figures

3.LIST OF TABLES

4. ABBREVIATIONS

APCs – Antigen Presenting Cells

COPD – Chronic Obstructive Pulmonary Disease

CQ - Chloroquine

CT – Computed Tomography

DC – Dendritic Cells

ECM - Extracellular Matrix

ELISA - enzyme-linked immunosorbent assay

FEV_1 – Forced Expiratory volume in 1 second

FVC – Forced Vital Capacity

HDM – House Dust Mite

IFNγ – Interferon gamma

IL-X – Interleukin - X

IP – Intraperitonial Injection

IQS – Injection Quality Score

LC3 – Light Chain 3

MMPs – Matrix Metalloproteinases

MRI – Magnetic Resonance Imaging

PET – Positron Emission Tomography

Th2 – T_2-helper cells

5. ABSTRACT

Allergic asthma is characterized by airway hyperresponsiveness and lung inflammation. To better understand disease pathophysiology, lung inflammation is monitored in animal models, and in this regard, non-invasive medical imaging is emerging for use in pre-clinical research. **The primary aim of this project is to develop protocols using non-invasive fluorescent optical imaging to quantitate lung inflammation in response to allergic challenge in a murine model of asthma.** For our studies, adult female BALB/c mice were repeatedly challenged with inhaled house dust mite (HDM) to induce "asthma". To assess the effectiveness of in vivo imaging in discriminating differences in inflammation, some animals were also treated with established and emerging anti-inflammatory agents (inhaled fluticasone, simvastatin, or chloroquine), or were subjected to allergen avoidance after initial HDM challenges. Fluorescent imaging in anesthetized, live mice was performed using an IVIS Spectrum Pre-clinical *In Vivo* Imaging System. A cathepsin-activated fluorescent probe, ProSense750, was delivered by a single tail vein injection to assess inflammation 24 and 48 hours after HDM challenge. Mice were fed an alfalfa free diet to reduce lung autofluorescence. For each experiment, we assessed the correlation between imaging data and total inflammatory cell count in bronchoalveolar lavage in each animal.

ProSense750 fluorescence in lungs was 2.8-fold higher in HDM challenged mice compared to allergen-naïve mice for up to 48-hours post-HDM. To account for signal variability we developed an Injection Quality Score (IQS) account for the degree of perivascular loss of ProSense750 with each injection. We tracked kinetics of lung fluorescence, performing imaging every six hours and found it to be maintained for up to 72 hours, with peak radiance 6-12 hours after injection. Addition of a second ProSense750 injection 24 hrs after an initial injection did

not augment peak fluorescence, thus for all studies we measured lung fluorescent 6-12 after a single dye injection. In HDM-challenged mice lung radiance strongly correlated with total lung cell count (r^2=9512); eosinophils (r^2=.8944); neutrophils (r^2=.9208); macrophages (r^2=.5497); and, lymphocytes (r^2=.9911). Interestingly, though allergen avoidance diminished lung inflammatory cell count, cathepsin-activated ProSense750 lung radiance was sustained. Fluticasone blunted ProSense750 lung radiance in HDM challenged mice, but this effect did not fully reach statistical significance suggesting residual cathepsin activity in the lung (p=.0548, one-way ANOVA). Simvastatin treatment reduced lung radiance and total cell counts by 77% in HDM challenged. Chloroquine (CQ), an autophagy inhibitor, had no impact on ProSense750 lung radiance but did reduce total BALF cell counts.

Our studies show that *in vivo* optical imaging provides a meaningful, non-invasive measure of lung inflammation, including dye specific enzymatic activity such as for cathepsins, in murine models of allergic asthma. This approach is a new option for repeated measurements in individual animals for drug testing and development.

6. LITERATURE REVIEW

6.1 Allergic Asthma

Asthma, as of 2013, affects more than 300 million people worldwide [1]. As one of the most prevalent airway complications there has been an increased interest to understand how asthma can be treated and the basis of the chronic inflammation that is associated with pathophysiology [2]. The majority of research has been focused on disease progression with significant emphasis on developing and leveraging insight in a variety of models of human airways disease. The inflammatory response associated with asthma is a prominent focal point for research. Persistent or uncontrolled inflammation underpins and is associated with the exacerbation of allergic asthma and has been a primary focus for developing new therapies [3]. Airway inflammation in asthma is also causally associated with development of airway remodeling that includes epithelial disruption and hypersecretion of mucous due to goblet cell hyperplasia, airway wall fibrosis, and smooth muscle layer hypertrophy. [3, 4]. The clinical manifestation of asthma includes shortness of breath and difficulty in breathing due to airway narrowing and increased airway resistance that is variably reversible [3, 4].

6.1.1 Pathophysiology of Allergic Asthma

Allergic asthma is characterized by hyperresponsiveness to an inhaled allergen which leads to an excessive inflammatory response, and that is manifest as excessive bronchial constriction in response to inhaled non-allergic stimuli [5]. Chronic inflammation in the airways underpins pathogenesis of remodeling in conducting airways (**Figure 1**).

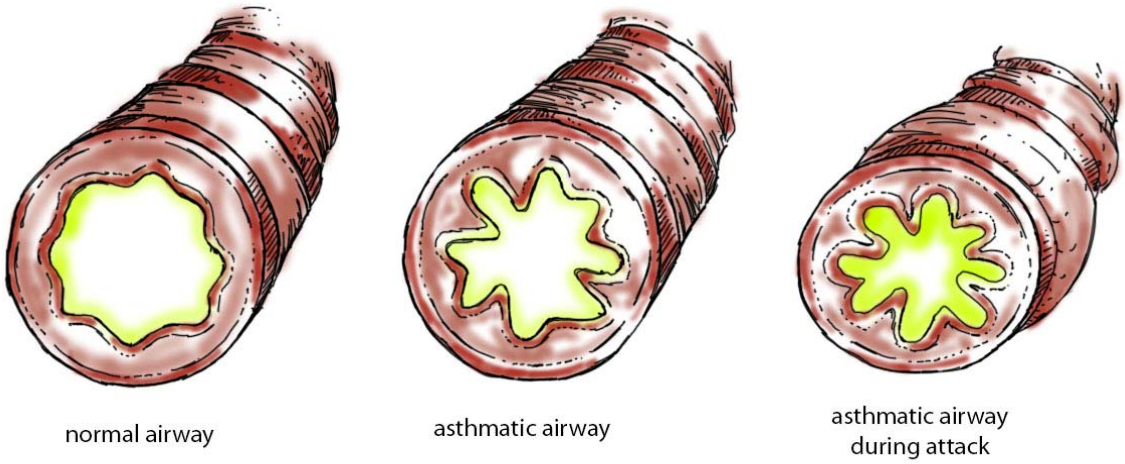

Figure 1: Narrowing of the airway lumen in diseased allergic asthmatic airways. During an asthmatic attack, a narrowing of the air occurs due to the inflammatory response associated with allergic inhalation.

Clinically, asthma primarily presents in patients as a reversible obstruction of airflow. Unlike chronic obstructive pulmonary disease (COPD), with asthma the obstruction in the bronchial system can be controlled (prevented) and reversed with inhaled therapies, including corticosteroids and β2-adrenergic agonists, respectively [6]. Patients typically present to clinic with difficulty in breathing, wheezing, dyspnea, and chest tightness symptoms [7, 8]. Diagnosis for asthma is most frequently confirmed using spirometry to measure lung function [9]. Diagnosis is confirmed when the FEV_1/FVC (forced expiratory air in one second / forced vital capacity, respectively) ratio is below 75% [10]. To differentiate between asthma and COPD, the patient is treated with an inhaled bronchodilator, typically a β2-agonst, and lung function is measured a shortly after; if treatment improves lung function (significant increase in the FEV1/FVC ratio), then an asthma diagnosis is confirmed [11].

At the cellular and molecular level, allergic asthma is characterized by an influx of immune cells into the bronchial airways which are responsible for secreting a milieu of cytokines (eg. IFNγ, TNFα, and IL-13 – more detail in *Section 6.1.2*), proteases, and other regulatory molecules [12-17]. Once secreted, cytokines and proteases modify the local microenvironment, in part, by affecting the bronchial cell types such as airway smooth muscle and bronchial epithelial layers [14, 18-20]. Airway smooth muscle hypercontractility is induced upon exposure to inflammatory mediators [21]; this phenotypic change underpinning excess airway narrowing and hyperresponsiveness that is at the root of asthma symptom manifestation [22]. To further pronounce this effect, multiple cytokines and growth factors associated with airway inflammation bind to airway smooth muscle cells and promote tissue hypertrophy, via cellular hyperplasia and hypertrophy, ultimately worsening reduced airflow associated with asthma "attacks" [21, 22]. The airway epithelium, which acts as a barrier between the outside air and the lung, can be "activated" by inflammation to drive the expression and release of cytokines, chemokines and other mediators that orchestrate and increase local inflammation and abrogates epithelial barrier function [3, 6]. Notably, a primary area of research focus is on how airway structural cells, including epithelial and airway smooth muscle, contribute to asthma pathogenesis through their secretory function to promote local inflammation and regulate tissue damage and repair (**Figure 2**) [23].

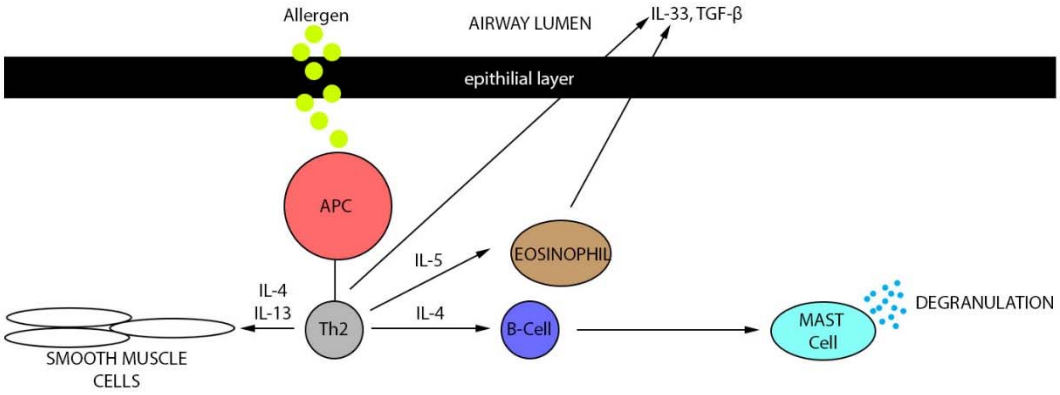

Figure 2: Inflammatory cytokine release associated with an asthmatic response. Allergen is inhaled through the epilithial layer of the lung. The allergen, which is considered a foreign substance through the inflammatory pathway. The allergen is taken up by an APC causing the secretion of interleukins and the activation T-helper cells eliciting the inflammatory response.

6.2 Immune Response in Allergic Asthma

The immune response in allergic asthma is a complex biological process that is orchestrated temporally and spatially by an array of different cytokines, pathways, and cell types [3, 24]. During an allergic asthma response, an allergen such as house dust mite, pollens, or fungi are inhaled and, coming into contact with the epithelial layer, induce receptor and non-receptor mediated pathways that induce a cascade of events that define the type and determine the magnitude of the inflammatory response. These include antigen-presenting dendritic cells that orchestrate innate immune response, as well as inflammation effector cells like mast cells, T-helper 2 (Th2) cells, and T regulatory cells [25]. Macrophages also play an important role in mediating the inflammatory response in asthma [26]. Macrophages are responsible for a large portion of the pro-inflammatory role which is associated with the cytokine release in the airways in asthma [27]. This cascade also orchestrates production and release of endogenous proteases

such as cathepsins that further contribute to the airway remodeling associated with allergic asthma [24]. A more comprehensive listing of cell types involved is included in **Table 1** [28].

Table 1: Cell types associated with inflammatory asthma

Cell Type	Function
T-Cells	Become activated when coming into contact with APCs. Involved in the innate immune response, activating other T-cells, removal of pathogen [29, 30].
Dendritic Cells	Secrete cytokines in response to antigen. Function in processing and presenting antigen on cell surface to elicit an immune response [31, 32].
Neutrophils	Ingests microorganisms and releases enzymes in the area of inflammation [33].
Eosinophils	Involved in the secretion of cytokines and proteases [34, 35]
Macrophages	Performs phagocytosis and removal of antigens and neutrophils during the inflammatory response [36].

Dendritic cells (DC) are responsible for the initiation of the allergic immune response, taking allergens, modifying and presenting it to Th2 cells which release a cascade of mediators that determine B-cell differentiation and function [37]. The Th2 cells are responsible for the activation of antibody synthesizing B-cells as well as releasing interleukins which have an effect on surrounding structural cells, including airway smooth muscle and epithelial cells [24, 38, 39]. During a subsequent exposure to the allergen, this cycle is repeated, however, it can occurs in a more pronounced manner that leads to a dysfunctional response that can trigger asthma episodes in susceptible individuals [24].

6.1.2 Cytokines, Proteases and Asthma

Two broad classes of mediators exist that contribute to asthma pathogenesis: cytokines and proteases [24, 40-42]. Cytokines are released via complex mechanisms that involve recruited lymphoid and myeloid cells such as T cell subtypes and mast cells as described above [24]. Their interaction with structural cells of the airway contribute in a primary manner to asthma pathophysiology [24]. An array of cytokines has been well described and linked to mechanisms that contribute to asthma progression [43-45]. For example, interleukin-13 (IL-13) is thought to play a key role in mediating airway hyperresonsiveness and airway obstruction [43]. This effect is likely associated with the capacity of IL-13 to induce secretion of other inflammatory mediators by the airway epithelium [46]. IL-4 is also an important mediator of airway inflammation by underpinning processes that lead to airway epithelial barrier dysfunction [47]. Furthermore, both IL-4 and IL-13 contribute directly to responses that lead to airway wall fibrosis associated with structural remodeling of the bronchial wall [46, 48].

Proteases can also contribute to airway remodeling and inflammation by changing the composition and structure of the extracellular matrix (ECM) surrounding airway smooth muscle cells and airway fibroblasts, as well as the lamina reticularis to which the epithelium is anchored [49]. Included among the different proteases present and secreted in association with airway inflammation, are the cathepsins [49, 50]. Cathepsins are a family of cysteine proteases that are enriched in lysosomes and can be induced for intra- and extra-cellular secretion by a number of stimuli and insults to support homeostatic protein breakdown and turnover. Cathepsins have been associated with physiological autophagy, apoptosis and the unfolded protein response [51].

Structurally, there are 15 known subtypes of cathepsins that differ on their genetic sequence. Each subtype has a tissue specificity that is associated with disparities in their

structure, catalytic mechanism and substrate in which they cleave [52]. A review by Vito et al. [53] compares the amino acid sequences between the different cathepsin sub-types showing large amount of conserved sequences between them. Cathepsin proteins include three distinct domains, namely L- and R- domains and the active site [53] The L-domain contains three distinct α-helices while the R-domain is primarily a β-barrel structure that are joined by a binding site . The active site includes residues that are conserved between different cathepsin subtypes, specifically Cys25 and His163 based on the cathepsin L template sequence [54].

Cathepsin production and activity has been associated with allergic asthma [24, 55]. Cathepsins are released from various antigen presenting cells (APCs) as well as eosinophils and neutrophils during an inflammatory response [50, 56]. Cathepsin release and activity is also linked to a variety of tissues and are associated with an number if chronic inflammatory and physiological conditions (**Table 2**) [41, 42, 52, 57]

Table 2:Sub-types of cathepsins associated with human disorders [53, 58-69].

Cathepsin Type	Associated Disorder	Primary Function
A	Galactosialidosis	Assists in transporting β-galactosidase and neuraminidase in the breakdown of sugar molecules.
B	Cancers and neurodegenerative disorders	Primarily used to enhance the proteolytic activity of other proteins
C	Papillon-Lefevre Disease, COPD, astham	Activation of serine proteases in inflammatory and immune cells
D	Breast cancer and Alzheimer's Disease	Protein turnover and proteolytic activation
E	Neuronal death and ischemia	Protein degradation and MHC class II pathway processing
F	Ceroid lipofuscinosis	Intracellular protein turnover
G	Blood-brain barrier breakdown	Intracellular pathogens and breaking down tissue during inflammation
H	Diabetes	Degradation of lysosomal protein
K	Osteoporosis	Bone remodeling and absorption
L	Myopathies and myocardial ischemia	Initiation of protein degradation
O	Cancer	Cellular protein degradation and turnover
S	Astrocytomas	Participation in protein degradation for MHC class II
V	Breast and rectal cancer, hypertrophy	Hydrolyzes proteins

During wound healing, tissue remodeling and inflammation several isoforms of cathepsins can be released which are tissue and process specific [53]. The role of cathepsins in allergic asthma has been of recent focus [24]. Specifically, cathepsin S is elevated in murine models of lung inflammation [70-72]. During an allergic response, pro-inflammatory markers such as IFNγ and IL-13 bind to APCs and other inflammatory cells which initiate a cascade response within the cell, including lysosome release and secretion of cathepsins [43, 72, 73]. Cathepsins then modify surrounding extracellular proteins, and also contribute to lung remodeling through activation of the apoptosis and autophagy pathways in structural cells [74].

6.1.3 Autophagy, asthma, and inflammation

Autophagy is a homeostatic catabolic process for macromolecular and organelle turnover and it can be further activated when cells are subjected to stress, for example, unfavorable environmental condition caused by nutrient starvation [75]. Through this process cells can replenish and maintain energy stores, as well as remove damaged or aged organelles to support survival and/or enable heightened metabolism when necessary (eg. acute and chronic biogenesis and release of ECM proteins or inflammatory mediators) [76]. During autophagy organelles and macromolecules are encapsulated in autophagosomes, which ultimately fuse with lysosomes to form autophagolysosomes [76]. Within autophagolysosomes, organelles and macromolecules are reduced to their simplest components in an acidic environment that activates lysosomal proteases (**Figure 3**) [75].

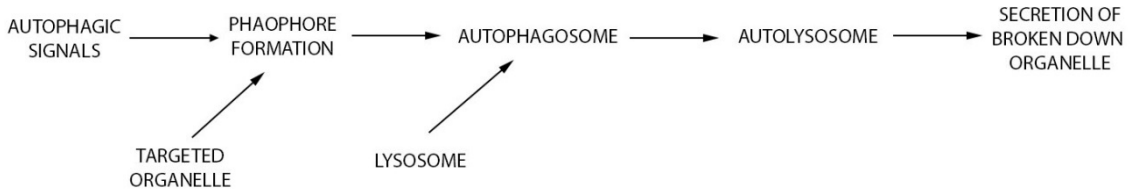

Figure 3:Autophagy Pathway. During autophagy, external signals triggers the formation of an autophagosome that has engulfed an organelle. The autophagosome merges with a lysosome which contains digestive enzymes that degrades the organelle into its molecular components.

By turning over constituents of cell organelles, autophagy promotes cell homeostasis and survival, under severe conditions [77]. However, excessive autophagy has also been linked to induction of pro-death pathways that lead to cell demise [78]. Due to this seemingly dual role, the precise contribution of autophagy in promoting or neutralizing pathogenesis of chronic and acute disease is not fully resolved [75, 76, 78].

In many disease states autophagy is associated with the pathophysiological process, including recent reports that suggest it may be a component of asthma pathobiology [79-81]. To date, there is insufficient data to ascribe a role, promotive or suppressive, for autophagy in asthma. Though autophagy activity occurs during airway inflammation and pathophysiology it has not been conclusively liked with promoting inflammation per se [76]. Some studies have described how autophagy is regulated and activated in airway smooth muscle cells due in response to exposure to pro-fibrotic and pro-inflammatory mediators [78, 82-84]. Based on the uncertainty for a role of autophagy in asthma, a tangential element of this thesis is to use in vivo imaging to monitor whether pharmacologic inhibition of autophagy affects allergen challenge-induced lung inflammation in mice.

6.3 Animal models of asthma

Animal models of human disease are vital tools to decipher complex pathogenesis mechanisms and for pre-clinical testing of emerging therapies. The majority of animal models for allergic asthma involve the use of mice as they offer a platform for effective genetic manipulation, exhibit immunological responses that mimic humans, and large numbers can be housed affordably and with ease [85, 86]. Despite these strengths, murine models of asthma do have some pivotal differences from the human lung and airway, and asthma's presentation: 1) mice have significantly fewer generations of conducting airways than humans, 2) the breathing rate of a mouse is almost double that of a human, 3) mice lack mucous glands, relying on airway epithelial goblet cells for mucous production, and 4) mice do not spontaneously acquire asthma, rather they mount an acute allergic response that generates an inflammatory signature that is similar to that seen in humans [86, 87]. With these caveats considered, research with murine

models of “allergic asthma” has been instrumental in describing fundamental immunologic and pathophysiologic processes associated with asthma.

As mice do not spontaneously generate asthma, protocols have been developed in which the animals are sensitized to, and/or aero-challenged with environmental allergens to elicit an “asthma-like” inflammatory response in the lungs [88-90]. Commonly used agents include ovalbumin, house dust mite or cockroach antigens, and fungal and ragweed extracts [91]. These can be injected to induce immune hypersensitivity and/or animals are subjected to inhalation challenge to promote lung-specific mucosal immune response, inflammation and tissue repair [92-95].

House dust mite (HDM) is commonly used as it is considered to be clinically relevant, being a very common trigger-allergen associated with human asthma [96-99]. When inhaled by mice, HDM acutely induces human asthma-like inflammation that is marked by significant eosinophilic infiltration and background neutrophilic infiltration that underpin the acquisition of airway hyperresponsiveness, a classic clinical hallmark of asthma [96, 100]. With chronic aero-challenge, HDM can also induce marked airway wall remodeling as is seen in long-duration human asthma [3].

Airway inflammation in murine models can be quantitated in a variety of ways to determine the degree and characteristics of allergen challenge-induced inflammation. The current “gold standard” is to perform immune cell counting and differential cell analysis in lung lavage. Typically, lymphocytes, neutrophils, eosinophils accumulate during the immune response, and the fractional abundance of alveolar macrophages decreased compared to baseline in allergen-naïve mice [101, 102]. Inflammation can also include multi-plex enzyme-linked immunosorbent assay (ELISA) to profile and quantify abundance of relevant cytokines, chemokines and growth

factors, as thus provide insight for molecular biomarkers of the inflammatory state in the lung [103, 104]. Lung histology is also routinely performed to assess the extent and spatial pattern of immune cell infiltration, however differential analysis of immune cell types is less reliable than can be achieved with manual light microscopy analyses or flow cytometry of lung lavage cell pellets [102]. While these procedures provide accurate assessment of lung inflammation, they are not without limitations, in particular they represent an experimental endpoint involving sacrifice of animals, thus cannot be used for repeated measurement in individual mice, mandating the use of many animals in order to track temporal changes in lung inflammation in chronic allergen challenge protocols.

For *in vivo* studies, several different murine strains have been used, including genetically engineered transgenic and gene knock out mice [88]. Each strain has its advantages and disadvantages, depending on the precise question(s) being considered [105-107]. One of the most commonly used strains is the BALB/c mouse which mounts a strong immune response and can exhibit significant airway hyperresponsiveness upon allergen challenge compared to other strains [108, 109]. For instance, BALB/c mice exhibit a strong Th2 cell response to inhaled allergen challenge, which parallels asthma pathophysiology in humans [110].

6.4 Non-invasive Imaging

Non-invasive imaging can be used in research to visualize and quantify structural features and/or spatial patterns of biological activity in different organs. While different imaging modalities have specific strengths and weaknesses, in general, they do enable real-time, temporal and spatial assessment of disease progression associated with changes in organ structure and

function [111]. Non-invasive imaging also allows for quantitation of disease progression without sacrifice, thus enabling repeat measurements over time in individual animals.

The lung is a spatially dynamic organ that continually moves in space during breathing. It also has relatively little tissue mass per unit volume compared to more dense organs (eg. bone) that are not air-filled. Thus, lung imaging focuses on measuring the physiological change on the lung compared to convention structural changes [112, 113]. Lung imaging and spatial co-registration of images in a living animal is particularly problematic due to the movement of lungs during breathing and because of the proximity of a beating heart. Different in vivo imaging approaches, such as lung magnetic resonance imaging (MRI) for example have relied on the development of protocols to compensate for this hurdle by using image registration techniques – identifying a landmark structure that determines when a particular imaging frame is recorded when the lungs are repeatedly in the same position during the respiratory cycle - in order to obtain in-focus images of highest possible resolution [112, 114, 115].

Magnetic resonance imaging provides high resolution scans of murine tissue by applying a magnetic field to align the spins of protons in the tissue, thereby generating a detectable signal [113]. Imaging of murine lungs with MRI has a number of challenges: 1) the lungs have minimal tissue density resulting in excess "noise" from air-filled space, 2) magnetic field irregularities occur at air-tissue interfaces, 3) the lung is a moving organ, and 4) cardiac motion also contributes to image blurring [116]. To obtain measurable images, researchers use fast gradient imaging sequences, spin-echo sequences that have been synced with the respiratory cycle, or hyperpolarized inhaled gas is employed [114, 117-119]. Another limitation is that MRI requires access to highly specialized equipment managed by a trained operator, thus is prohibitive to many investigators.

Positron emission tomography (PET) is a nuclear medicine imagine technique that has been used to study lung physiology and pathophysiology [120, 121]. PET has also been used to measure murine lung inflammation using positron-emitting isotopes [122]. While PET scans can provide excellent insight into metabolic processes of the body, it too has its own set of complications: 1) spatial resolution due to the small size of the mouse thorax, 2) usage of radioactive injectable agents, and 3) the amount of radioactive signal being detected versus emitted [120, 121, 123]. As with MRI, PET use is also limited by access to highly specialized equipment that is managed by a trained operator.

Micro computed tomography (CT) has been a gold standard for non-invasive imaging of the lung in a clinical and basic science setting [115]. Micro CT utilizes x-rays to develop a series of image planes that can be reconstituted to generate a stack of two-dimensional images through the entire lungs. Micro CT is widely used to track physiological changes in lung morphology rather than measuring biological activity such as inflammation. Some attempts have been made at merging micro CT with other imaging modalities that track biological function, such as fluorescence optical imaging, to create structural and functional images of disease progression. The main limitations in using micro CT imaging for the lung include it having poor soft tissue imaging capacities and that it requires exposure to damaging high energy x-rays, precluding its repeated use in individual animals [124-126]. Micro CT imaging also requires access to highly specialized equipment that is managed by a trained operator.

6.4.1 Optical Imaging

Optical imaging is a non-invasive technique that detects the visible light and infrared electromagnetic spectrum for spatial characterization and, with an appropriate dye, can be used

to quantify the magnitude and nature of biological activity associated with a process of interest (eg. inflammation) [127]. A unique strength of optical imaging comes from the unique and diverse properties of injectable agents that can be activated in situ [128-130]. This potential can relatively easily be exploited and optical imaging technology is relatively simple – computer controlled light source, detector and camera – and a breadth of enzyme-activated dyes are available commercially [128-131]. For these reasons optical imaging is gaining popularity for non-invasive assessment of process such as inflammation in tissues of small animal disease models. As noted in a previous section, optical imaging approaches are also suitable for simultaneous imaging in conjunction with other imaging technologies. For instance, it has been used in conjunction with micro CT to merge image and enable spatial segregation of biological activity (eg. cathepsin activity) so that activity can be directly associated with sites of tissue remodeling [132].

Fluorescent imaging is a sub-modality of optical imaging that is enabled by the use of an injectable dye/contrast agent that includes a high intensity fluorochrome that absorbs light of defined wavelength and has a narrow emission spectrum [133]. A common design is for such contrast agents to be "activatable", as in a pre-state they are either not strongly fluorescent or have a unique emission spectrum compared to the activated-state when can be highly fluorescent with a emission spectrum that is distinct from that of the pre-state dye (described in subsequent Section 6.5). Activation is frequently based on capacity for the selective cleavage of the dye molecule, for example a peptide linker of defined sequence, by a specific enzyme or enzyme class (eg. cathepsins, matrix metalloproteinases). This design enables the quantification of the signal such that as more dye is activated, the magnitude more signal is generated in direct correlation with the level of enzyme activity [134, 135]. Advances in chemical and molecular

engineering to develop contrast agents with defined excitation and emission spectra, thus enabling discrimination for natural auto-fluorescence has been critical in enabling wider use of *in vivo* optical imaging in biomedical research.

Fluorescence imaging has long been applied for broad use in microscopy applications of cells and tissue sections that provide a static sample that typically is less than 200μM in depth [133, 136-138]. With development of *in vivo* optical imaging technology (described in more detail in the next section), major technology hurdles that have been solved relate to need to localize a signal in space in specific internal tissues (eg. heart) that can be >1cm from the body surface in a small animal, and are often also obscured by dense structures or tissue layers (eg. ribs, skin, hair) present between the imaging detector and the organ of interest. As such, to date *in vivo* optical imaging has chiefly been standardized for monitoring larger and more superficial structures, for example tracking growth of primary tumors and the formation of secondary tumors in animal cancer models [139]. Imaging of deeper organs is subject to significant refraction and absorption of light by other organs and structures that interferes with detection and spatial resolution of the signal of interest [111, 140].

Imaging organs within the thorax is made difficult by confounding effects of the surrounding ribcage and muscle layers that refract light [112, 141]. Thus, regardless of the imaging modality, the lungs pose a number of technical hurdles that can hamper imaging. In summary these include: 1) the lungs being air-filled and with a low proportion of tissue per unit volume, being composed of a web thin interstitial structures that are difficult to resolve using imaging; 2) the lungs are located in the thoracic cavity which is demarcated by a bony rib cage and dense muscle that refract and absorb electromagnetic signals; and, 3) in living animals the lungs are not stationary, rather move and change shape and size constantly with breathing,

making it difficult to obtain high resolution images [112]. These difficulties are compounded when imaging is being carried out in a small animal such as a mouse in which the breathing rate is very rapid [140, 142].

In order to circumvent technical challenges associated with optical imaging two sub-modalities of fluorescent can be used in small animals such as mice; epi-illumination and trans-illumination. These approaches differ in the position of the excitation light source in relation to the animal (**Figure 4**).

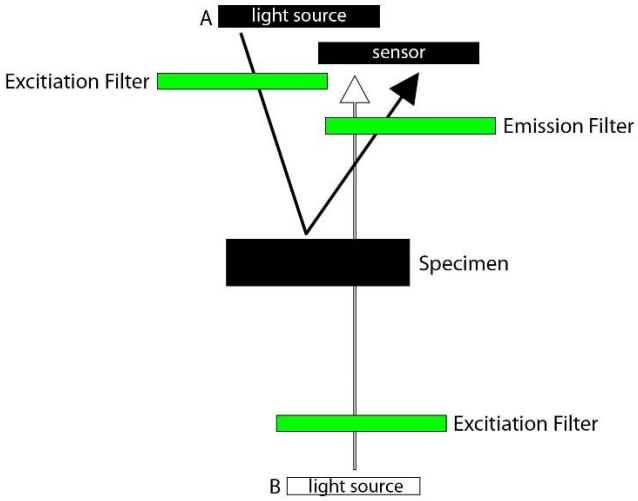

Figure 4: IVIS In vivo fluorescent imaging chamber light sources. The IVIS In vivo fluorescent imaging chamber has two sources of light. A) Epi-illumination uses light refracted off the mouse and uses sensors on the same size to measure. (black arrow) B) Trans-illumination passes the light through the specimen and has sensors to collect the light on the opposite side. (white arrow)

For epi-illumination an excitation light source is positioned above and at some distance (centimeters) from the animal, and emission light detectors are also positioned above and centimeters away from the animal. Due to the nature of the excitation and emission collection technique, epi-illumination is the approach of choice for surface organ imaging, but has limited sensitivity and resolution for deep tissue imaging. During trans-illumination the excitation light

source is beneath and very near the animal to prevent reflection from skin and outer body structures. For trans-illumination emission light detectors are positioned above and at some distance (centimeters) from the animal to capture emission signal generated by excitation light applied beneath the animal. Trans-illumination is the imaging method of choice for deep tissue imaging [143, 144]

6.5 Fluorescent imaging agents

Tissue autofluorescence is a natural characteristic of tissues and biological fluids [145-149]. Thus, to selectively detect fluorescence signals that are an index of biological function or presence of a particular mediator *in vivo* requires the use of an agent with specific fluorescence excitation and emission properties that can be activated and selectively detected when needed [135]. The dyes are designed to be delivered by vascular injection, typically through the tail vein, several minutes to hours prior to imaging, and have a post-activation half-life of approximately 4 hours. To avoid the depletion of dye during the measurement window, thus preventing maximum fluorescence to be achieved, the absolute dose of dye injected must be high enough to avoid signal blunting; this must typically be determined empirically as there is significant variation between animals, disease models, and during the disease cycle in longer duration protocols.

Many fluorescent indicators for enzyme activation have been developed for optical imaging research applications [131, 150]. For example, the ProSense 750 that I used for my studies, as it is selectively activated by cysteine proteases (cathepsins), which are released by immune cells and accumulate in the lungs in response to allergen challenge, as well as being released by structural cells of the lung in response to cytokines and growth factors [109, 151]. **Figure 5** depicts a generic injectable peptide-backbone fluorescent probe.

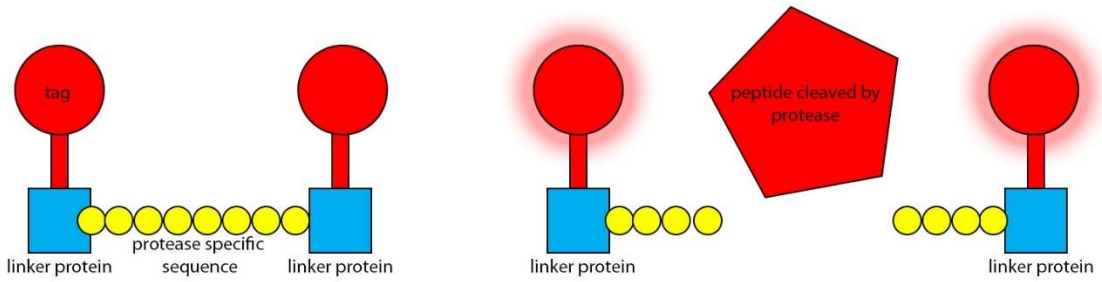

Figure 5: Generic fluorescent probe structure and activation. Fluorescent probes have a protease specific peptide backbone connected by two linker proteins. The Linker proteins are also connected to the fluorescent tags. When near, the reporter tags quench one another resulting in no signal. However, when a protease recognized and cleaves the peptide backbone, the two fluorescent tags are separated resulting in the tracer to emit a detectable signal.

The dye consists of two parts: a reporter molecule(s) (a fluorochrome) and linker peptide. Reporter molecules are linked by a peptide of defined amino acid sequence that mimics catalytic targets for different enzyme classes, for instance a protease such as cathepsin. Once cleaved, the two reporter molecules, which quench mutual fluorescence in the intact probe due their close proximity, become spatially separated, thus enabling fluorescence emission that can be monitored while target tissues are illuminated with an appropriate light excitation signal (**Figure 5**) [152, 153]. In such a case the amount of probe that is cleaved directly reflects the level of activation of the protease in the organ or tissue of interest and this is manifest as greater fluorescence radiance, as measured by a photodetector.

A wide spectrum of dyes with defined fluorescence properties that are activated by biological process such as bacterial infection progression, apoptosis, tumor growth and metastasis, neutrophil elastase activity, matrix metalloproteinase activation, and angiogenesis are commercially available for pre-clinical research in small animal models to track induction and pathogenesis of disease. In these cases, the indicator acts as a contrast agent, and is designed to

be modified by cell or tissue-specific enzymes, mediators or binding interaction with endogenous molecules. Based on biological evidence, optical imaging protocols can be designed to reveal the location and magnitude of activity related to a particular pathophysiological process (eg. inflammation, apoptosis) that is ascribed to specific cell types, in individual structures (eg. tumor or blood vessel). As the fluorescent dye can be activated by pathways associated with disease processes, changes in individual pathways can be quantified repeatedly over time to track disease phenotype progression in individual animals [151]. This is achieved by selective detection and quantitation of the intensity, position and size of the area of the radiance in tissues [109, 111, 140, 154]. There is significant effort in developing near infrared probes as autofluorescence is relatively low in this range of the electromagnetic spectrum, and higher frequency infrared light is better able to pass through tissues [155].

7. HYPOTHESIS AND AIMS

As asthma has reached near epidemic levels worldwide, there is a significant need to understand pathophysiology and streamline new drug development and testing. As such there is increased focus on using new technologies, including non-invasive imaging in suitable animal disease models, to promote translation of basic research through pre-clinical testing and to rapidly screen new compounds as therapeutics. With respect to murine models of asthma, costs and efficiency limit screening, and there is potential for hurdles, but this can be greatly mitigated using protocols that include repeated measures in individual animals. Such capacity would enable the leverage of potential that transgenic and/or knockout mouse models offer. For one, non-invasive imaging offers the opportunity for repeated measures in individual mice to reduce variability, enable more robust assessment of long term effects of interventions, and more effectively assess whether novel compounds can reverse established disease.

Allergic asthma is a chronic inflammatory disorder that is triggered and exacerbated by exposure to allergic, inhaled or systemic [4]. Inflammation includes the influx of leukocytes – chiefly eosinophils, neutrophils and lymphocytes - to the lungs, thus promoting pathophysiology [18, 19]. These cells mediate their effects by secreting a myriad of protein and lipid-based mediators, including cytokines, chemokines, growth factors and proteases that underpin sustained inflammation and orchestrate local responses that contribute to tissue remodeling [156]. Cathepsins are cysteine proteases that have become a recent focus for research, with evidence that they regulate ECM remodeling of asthma [51, 72], a process that progresses through cycles of damage and repair associated with immune cell recruitment [52].

My project is designed to test the utility of non-invasive fluorescent optical imaging, using a cathepsin-activated dye, comparing differences in lung radiance in allergen-naïve and allergen challenged mice, as well as assessing the impact of anti-inflammatory therapies in allergen challenged mice. **The primary aim of this project is to develop protocols using non-invasive fluorescent optical imaging to quantitate lung inflammation in response to an allergic challenge in a murine model of asthma.** Specifically, for my experiments, cathepsin-activated ProSense® 750 *in vivo* fluorescent imaging agent with an excitation and emission wavelength at 750 and 770 nm respectively was used. [109]. The utility of this dye as an index of lung inflammation has been validated, as the degree of fluorescence activation correlates with cathepsin expression in a LPS-challenge mouse model [157]. The work in my thesis applies *in vivo* optical imaging in a house dust mite (HDM) challenge murine model of allergic asthma to determine whether it can support pre-clinical assessment of allergic inflammation, with quantitative comparisons of multiple treatment groups.

For my studies I employ an already-established murine model of allergic asthma, replying on repeated intranasal challenge with HDM lysate [82, 158]. The HDM challenge model is considered to be clinically relevant as HDM is a principal aero-allergen for allergic asthma, and many pathophysiologic features mimic clinical presentation of asthma, including lung inflammation (influx of eosinophils, neutrophils and macrophages) that includes accumulation of cytokines and proteases, and the development of reversible airway hyperresponsiveness [26, 27, 91].

This project is designed to develop, test and validate a working protocol for using fluorescent optical imaging to quantitate the lung inflammatory response associated with allergen challenge. **We test the overarching hypothesis that in vivo optical imaging using fluorescent**

tags can effectively measure and track the allergic inflammatory response in the lung of allergen challenged mice. To test the hypothesis I set out two Specific Aims:

Specific Aim 1): *Utilize the IVIS® series pre-clinical in vivo imaging system to create and test a technical protocol to monitor and quantitate inflammation in the lung in HDM-challenged mice, comparing to allergen-naïve mice.* This series of studies creates a platform that can support ongoing and future pre-clinical research but solving technical issues, optimizing the image collection process, establishing image processing and capture protocols, and refining methods to normalize data to reduce variability and enable comparisons between groups.

Specific Aim 2): *Test and validate the optical imaging protocol I develop in Aim 1 to quantify responses to asthma therapies that inhibit the inflammatory response, using a pre-clinical drug testing design.* These studies provide real-world assessment of the applicability and potential utility of the *in vivo* optical imaging protocol and platform I establish in Aim 1. Experiments will also provide new insight about cathepsin biology and involvement in lung inflammation, pathophysiology and pathobiology (eg. autophagy).

8. METHODS

8.1 Murine Model

8-week old female BALB/c mice (GMC, University of Manitoba, Winnipeg, Manitoba, Canada) were used as the experimental animal model. All animals were housed in polycarbonate cages in a controlled environment at the University of Manitoba's Animal Care Facility. Mice had access to food and water *ad libitum*. Upon arrival at the facility, mice were given a one-week acclimatization period prior to being recruited into the HDM challenge protocol. All animal procedures were approved by the University of Manitoba Animal Ethics Committee as outlined by the Canadian Council on Animal Care

8.2 Allergic Asthma Challenge/Treatment Models

All mice were on an alfalfa-free diet (Harlan Laboratories, United States of America) to reduce auto-fluorescence, with the exception that a control group fed regular mouse-chow was included in one study. To induce allergic lung inflammation, mice underwent an acute, 2-week HDM challenge as outlined in **Figure 6**.

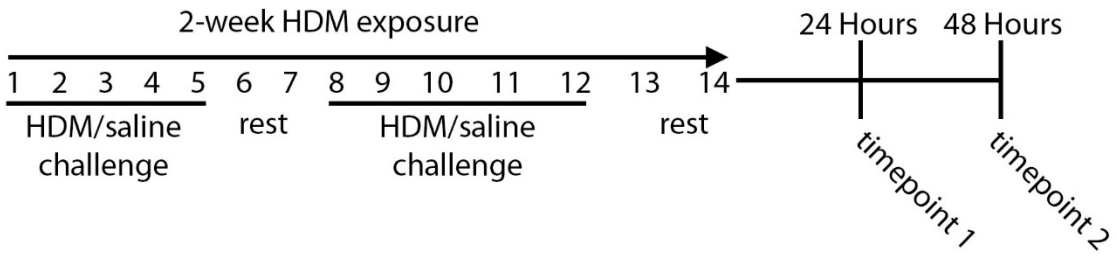

Figure 6: Graph of the two week acute allergen exposure model for 8 week old BALB/c mice. The timeline provides indicates the duration of HDM exposure, as well as the typical experimental time points (24 and 48hrs after final HDM challenge) that were employed throughout this project. During two weeks HDM exposure, allergen was delivered intra-nasally for 5 consecutive days, than an additional 5 days with a 2 day "rest" in between using HDM in a formulation outlined in Methods.

Mice had five days of intranasal HDM challenge followed by two days' rest for a total of 14 days repeat. The challenge consisted of HDM (Greer Laboratories, Lenoir, North Carolina, United States) dissolved in hospital grade saline at a concentration of 2.5mg/mL. The cocktail was delivered via pipette tip intranasal while the mice were under 4% isoflurane anesthesia. For some studies mice were given an intranasal combination of HDM/simvastatin (Toronto Research Chemicals, Toronto, Ontario, Canada) or HDM/fluticasone propionate (gift from GlaxoSmithKline Canada Inc, Mississauga, Ontario, Canada). When used, simvastatin was delivered at a concentration of 6mg/kg, 3mg/kg or 1.5mg/kg, and fluticasone propionate was delivered at a dose of 10µg/kg. In other studies mice were also treated with the autophagy inhibitor, chloroquine (CQ) (Sigma-Aldrich, Toronto, Ontario, Canada) alone or in combination with HDM challenge. In these studies CQ was delivered by interperitonial (IP) injection (50 mg/mL) in conjunction to the HDM challenge.

8.3 In Vivo Fluorescent Imaging

Fluorescent imaging was performed using the IVIS Spectrum Pre-clinical *In Vivo* Imaging System (IVIS) (Perkin Elmer, Waltham, Massaschusetts, United States). Mice were initially anesthetized using 4% isoflurane gas, then anesthesia was maintained throughout imaging using 2.5% isoflurane delivered by a nose cone in the imaging instrument. Prior to imaging mice were injected via tail vein with 100µL of ProSense®750 (Perkin Elmer, Waltham, Massachusetts, United States) at a concentration of 4nmol as per manufacturer's instructions. Mice were placed on the imaging stage with ventral side facing up with their upper limbs tapped down to minimize light travel distance. Image collection and analysis was performed using the Living Image Software, version 4.4 (Perkin Elmer, Waltham, Massachusetts, United States) by a single observer (ML). Mice were imaged using trans-illumination at an excitation wavelength of 745nm and emission wavelength of 780nm, using exposure times from 0.5 seconds to 1.5 seconds at 0.25 second intervals, with an f/stop of 1 or 2, lamp level set at high or low level, and medium binning selected for image processing. In total, 20 images were obtained per mouse per experimental time point. The mouse chest region is isolated using the imaging software and fluorescents is calculated.

8.4 Bronchoalveolar Lavage

At the completion of each study (ie. allergen challenge, in vivo imaging at multiple experimental time points, and measurement of lung function), mice were anesthetized using IP injection of 100µl pentobarbital sodium (54.7 mg/mL) (McGill University, Montreal, Quebec, Canada). Bronchoalveolar lavage was collected by twice flushing lungs with of ice-cold saline delivered by syringe through an intratracheal tube, 1 ml at a time. The lavage was stored on ice

then centrifuged (1000 rpm, 10 minutes) to pellet cells. Supernatant was collected and frozen at -80ºC for future cytokine analysis, whereas the cell pellet was resuspended in 1mL of cold saline then subjected to total cell counting: calculated by placing 10µL of the re-suspended cells on a hemocytometer, and counting cells in three random fields to obtain an average cell count.

To determine immune cell differential composition, re-suspended cells were subjected to cytospinning onto glass microscope slides (100µL of cell suspension; 5 minutes, 1000rpm). Slides were dried in room air for 20 minutes, then stained using Fisher Heathcare™ PROTOCOL™ Hema 3™ Manuel Staining Solution (Fisher Scientific, Waltham, Massachusetts, United States) as per manufacturer's instruction and our established protocols [102]. After mounting a coverslip we determined the number of eosinophils, neutrophils, macrophages, and lymphocytes by manual counting, based on morphological features as we have described [102]. Cell counts for each animal were averaged from counts of six random fields of view per slide.

8.5 Cell Culture – treatment with autophagy inhibitors and activators

Human airway smooth muscle primary cultures previously established in our group [159, 160] were generated from resected 3rd-5th generation conducting airway specimens of consenting donors who underwent thoracic surgery at the Health Sciences Centre, Section of Thoracic Surgery as per protocol approved by the Human Research Ethics Committee, University of Manitoba. Cryopreserved vials of cells were thawed and gown in 100mm dishes using Dulbecco's Modified Eagle's Medium (DMEM) (Gibco Life Technologies, Burlington, Ontario) supplemented with 10% Fetal Bovine Serum (FBS) (Gibco Life Technologies, Burlington, Ontario) and 5% penicillin/streptomycin (Gibco by Life Technologies, Burlington, Ontario).

Cells were plated at passage 2, and used at passage number 4-5, having employed a passage a split ratio of 1:4. For experimental protocols cells were grow to ~70% confluence, then media was changed to one of the following 5 conditions for subsequent collection of total protein lysates 0-96hrs thereafter:

a) *negative control*: DMEM;

b) *"cytomix" treatment*: DMEM supplemented with 10ng/mL each of tumor necrosis factor α (TNF-α), interleukin 1β (IL-1β), and interferon γ (IFN-γ)(PeproTech, Quebec, Canada);

e) *positive control:* DMEM supplemented with the autophagy inducer, rapamycin (1μM) (Sigma-Aldrich, Toronto, Ontario, Canada).

8.6 Western Blot Analysis

Total protein cell lysates from individual 100mm culture plates was collected from primary human airway smooth muscle cell cultures subjected to negative control, cytomix, cytomix/Baf-A1, cytomix/3-MA or positive control conditions were collected at 0, 24, 48, 72, and 96 hours treatment in 200μL of RIPA buffer (Aqueous solution with 10 mM Tris pH 7.5, 150 mM NaCl, 1:100 NP40, 1g/100mL Deoxycholic Acid Salt, 0.1% SDS, 1:100 protease inhibitor cocktail (Sigma-Aldrich, St. Luuis, MO), 1:100 phosphatase inhibitor cocktail 2 (Sigma-Aldrich, St. Louis, MO), and 1 mM PMSF, pH adjusted to 8.0). Total relative protein concentration in cell lysates was measured using a BioRad DC-Assay Kit (based on the Lowry method) (BioRad, Mississauga, Ontario) using bovine serum albumin to generate a standard curve with minimum correlation of r^2>.95 being acceptable. Thereafter, in preparation of SDS-polyacrylamide gel electrophoresis (SDS-PAGE), lysates were diluted to 1μg/μL concentration using a denaturing loading buffer containing sodium dodecyl sulfate (SDS) and β-mercaptoethanol as we have

described [102, 161]. Proteins were size fractioned using 15% SDS-PAGE and thereafter electro-transferred to nitrocellulose membranes by wet transfer as we have described. Membranes were then blocked for one-hour using cold 10mM Tris buffered saline containing 0.1% Tween 20 (TBST) supplemented with 5% (w/v) dry milk powder. After washing with TBST membranes were incubated overnight at 4°C in TBST/1% milk powder containing mouse monoclonal primary antibodies for autophagy markers: Light Chain 3 (LC3)-β (dilution 1:500) (Sigma-Aldrich, Toronto, Ontario), or the autophagy gene (ATG) 5/12 complex (dilution 1:250) (Cell Signaling Technology, Danvers, Massachusetts). To develop blots, membranes were rinsed in TBST then incubated for 1 hour at room temperature in TBST containing rabbit anti-mouse Ig (1:1000). After a final wash with TBST, blots were developed on autoradiographic film using enhanced chemiluminesence (ECL) reagents (GE Life Sciences, Toronto, Ontario, Canada) as per manufacturer's protocol. On all blots we also probed from β-actin to be used as a loading control. Blots were imaged using a page scanner and Image Lab software (BioRad, Mississauga, Ontario).

8.7 Statistical Analysis

Statistical analysis was performed on data using GraphPad Prism 5 (La Jolla, California, United States v5.03). Student t-test and ANOVA analysis was performed as outlined in experimental results and Figure Legends. A p-value of $<.05$ was considered significant.

9. RESULTS

9.1 Optimization of Imaging

8-week old female Balb/c mice underwent 2-weeks HDM intranasal challenge, and we first determined whether diet was a determinant of autofluorescence. For this study mice were fed a diet of wither regular mouse chow, or a diet of mouse chow that is alfalfa-free. We first determined the detectable levels of basal autofluorescence using threshold parameters of the IVIS optical imager for trans-illumination image detection, exposure time, illumination point number, and wavelength. Mice that were fed regular chow had significantly higher levels of autofluorescence compared to mice on an alfalfa-free diet for two weeks, in which autofluorescence frequently exists at a level below detectable limits **(Figure 7)**.

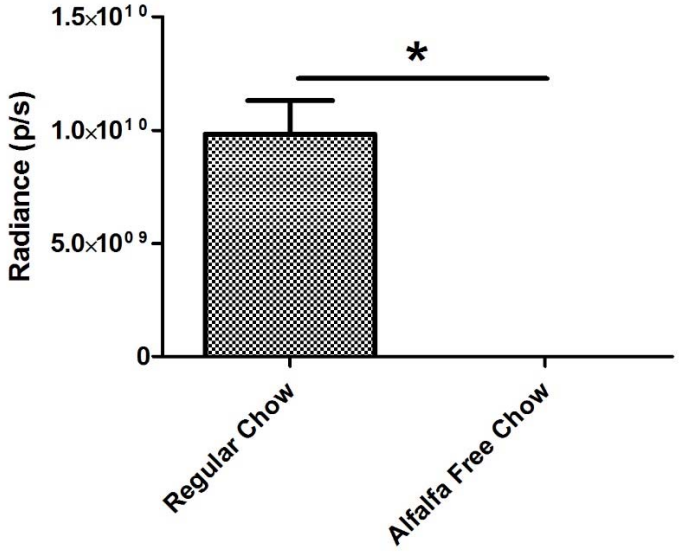

Figure 7: Comparison of autofluorescence in the thorax of mice fed either regular chow or alfalfa-free chow for two weeks. Images were captured using threshold image capture settings with the IVIS Optical Imager (1 sec, exposure | 2 f/stop | lamp level, high). No contrast agent was injected in the animals. Error bars represent SEM of data obtained in one measurement from three different mice. * = $p<0.05$ as per Student's T-test.

Thus, feeding mice an alfalfa-free diet markedly dampened autofluorescence to levels below the detectable range (ie. equivalent to 0), whereas mice on a regular chow diet (that includes alfalfa) exhibited an average florescence of $1x10^{10} \pm 2.489x10^{009}$ p/s.

We next determined the extent to which the 2-week HDM intranasal challenge protocol could induce lung inflammation that is associated with cathepsin-dependent activation of ProSense750 **(Figure 8)**.

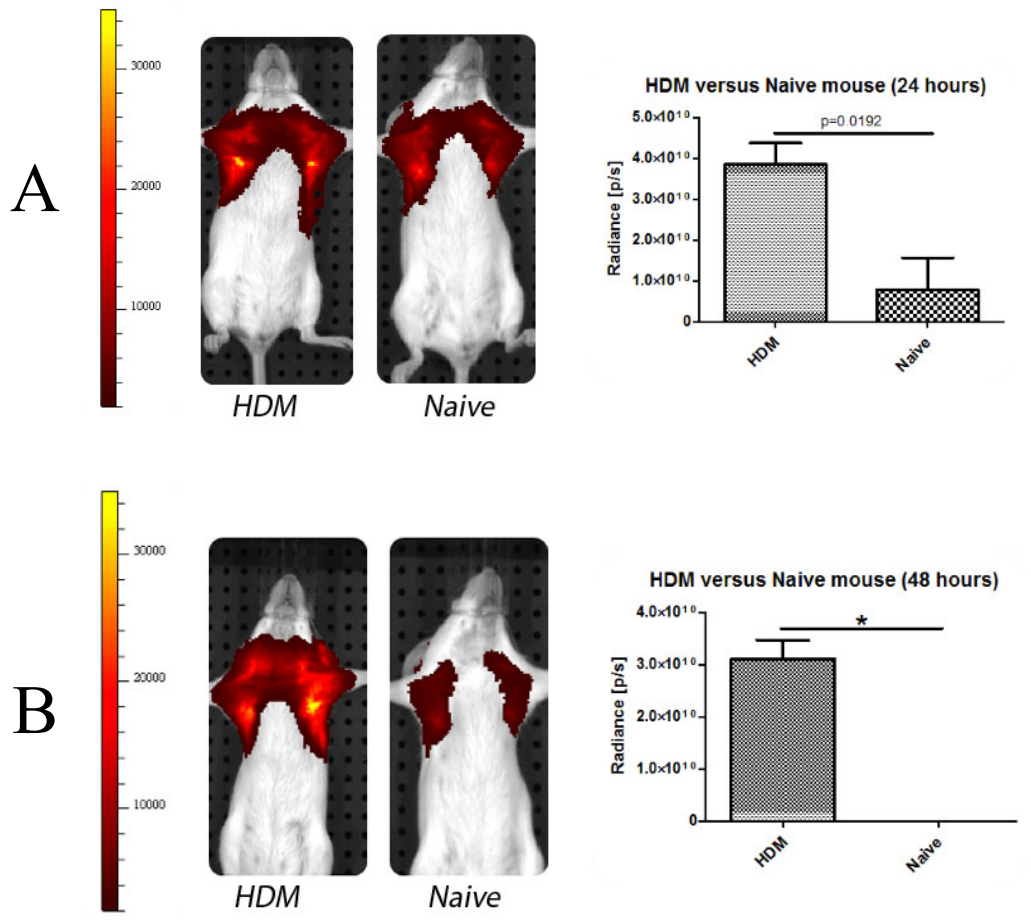

Figure 8: ProSense 750 activation and lung radiance induced by 2-weeks of HDM challenge. Six mice were subjected to acute HDM intranasal challenge protocol; 18 hours after final allergen challenge mice received a tail vein injection of ProSense 750 as decried in Methods. Optical imaging in trans-illumination mode (excitation wavelength 745nm; Emission wavelength: 780nm), was performed 24 and 48 hours after final HDM challenge in each mouse. A) 24 hours post allergen challenge (6 hours post ProSense 750 injection): left panel shows a typical whole body image for an HDM-challenged and allergen naïve mouse (0.5 sec exposure | f/stop 2 | lamp level low). Bar on the left indicates pseudocolored scale for radiance. Histogram

shows mean ± SEM of lung radiance from 6 mice. B) 28 hours post allergen challenge (30 hours post ProSense 750 injection): left panel shows a typical whole body image for an HDM-challenged and allergen naïve mouse (0.5 sec exposure | f/stop 2 | lamp level low). Bar on the left indicates pseudocolored scale for radiance. Histogram shows mean ± SEM of lung radiance from 6 mice. Mean values were compared between HDM-challenge and allergen-naive groups at each time point using Student's T-test. *P<0.05 (0.0192 for 24 hr time point as indicated).

For imaging at two experimental time points (24 and 48h hours post allergen challenge), mice received a tail vein injection of ProSense750 18 hours after final HDM challenge (ie. 6 hrs and 30 hrs prior to imaging at 24 and 48 hours post-allergen, respectively). We measured marked radiance of ProSense750 in the lungs of mice at both 24 and 48 hours post-allergen challenge. The radiance 24 hours after allergen challenge **(Figure 8A)** was 25% higher than that we measured 48 hours after allergen challenge **(Figure 8B)**; this may be due to loss of dye bioavailability, changing character of inflammation, or both. We did detect basal ProSense750 radiance in the lungs of allergen naïve mice 6 hours after dye injection (24 hour experimental time point), this signal was not detectable 30 hours after dye injection (48 hour experimental time point), suggesting that bioavailability of ProSense750 was compromised at the later time point. At the completion of imaging at 48 hours, to confirm that the chest radiance for ProSense750 was principally generated in the lungs, for three mice we performed one additional imaging analysis in intact lungs that were excised from each animal. We compared the radiance in the excised lung to what we measured in the chest of the same animal in vivo. We confirmed that normalized radiance was not significantly different from what we measured *in vivo* for either HDM-challenged or allergen-naïve animals (P=0.15 for both HDM- and naïve-mice; Student's T-test, n=3).

9.2 Injection Quality

We next determined whether the quality of the injection of ProSense750 dye into the tail vein played a role in the magnitude of lung radiance that we subsequently measured in the chest in vivo. In order to assess the efficiency of tail vein injection, we tracked tail vein radiance after injection. We obtained images from the tip to the base of the tail on both sides with *a priori* rationale that injection quality is proportional to the efficiency of delivery directly to the vein, without loss into perivascular regions surrounding the injection site. Low quality (efficiency) tail vein injections would thus be characterized by more pronounced pooling of dye in tissues surrounding the injection site, resulting in less effective systemic delivery of ProSense750, including to the lungs.

To enable semi-quantitative assessment of injection quality, we developed a numerical scale from 1 to 3 based on: the number of injection attempts; the radiance that was measurable in the vein; and, the radiance of dye measured in perivascular regions at the injection site. **Table 3** summarizes the parameters for the injection quality assessment scale and how injection quality scoring was allocated.

Table 3: Injection quality assessment scale.

Group	Parameters
1	One to two injections single side, minimal in perivascular region
2	One to two injections per side, approximately half dye is in perivascular region
3	Three to four injection attempts per side, majority of the dye is in the perivascular space

For this study we performed injections of ProSense750 in 10 naïve mice and used the quality assessment criteria to assign an injection quality score. **Figure 9** summarized the results of the injection assessment analysis, and shows that chest radiance was unaffected if injection

quality was scored between 1 and 3, this did not reach statistical significance (P>0.05, one way ANOVA).

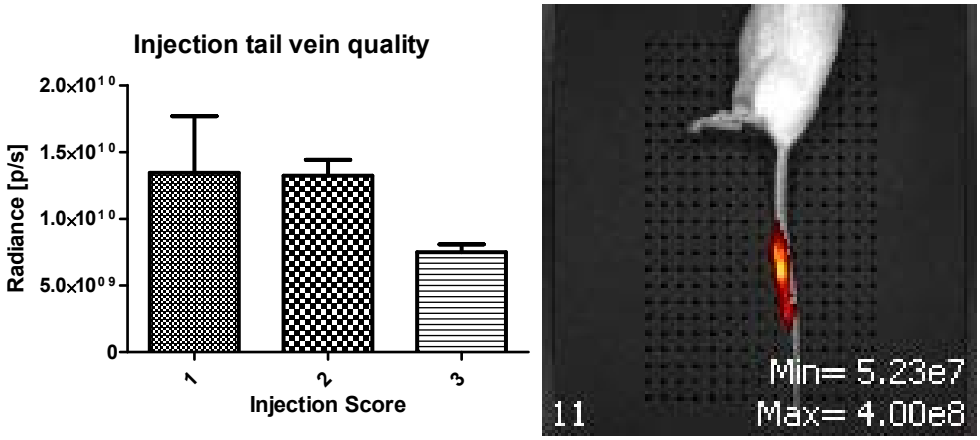

Figure 9: Assessment of quality of tail vein injection of ProSense750. Allergen-naïve mice were subjected to tail injection and full tail imaging was commenced within 10 seconds. Based on criteria described in Table 3, each injection was scored. Chest radiance was measured 6 hours after ProSense750 injection. (A) Correlation of chest radiance (Y-axis) with tail vein injection score (X axis).Tail vain quality score was binned. The number of injections included in each bin were: Score 1 (2); Score 2 (4), and Score 3 (5). NO significant difference was apparent in chest radiance between groups (One Way ANOVA, P>0.05). (B) Typical IVIS image showing vein and perivascular dye radiance immediately after a tail vein injection (imaging set up: 1 sec exp | f/stop 2 | lamp level low). The example shown is a injection quality score of 1.

Based on the results for this pilot quality control study, for all experiments in this project, only data from animals with an injection score between 1 and 2 were used for *post hoc* analyses.

9.3 PS750 Kinetics

We next assessed the kinetics for dye accumulation and activation in the lungs post injection, as well as tracking the duration over which ProSense750 signal was sustained in the lungs of allergen-naïve and HDM-challenged mice. This understanding is necessary to identify the optimal window for measuring lung radiance in experiments that test the utility of ProSense750 and IVIV optical imaging to measure allergic lung inflammation and the effects of

therapeutic interventions. As described in the sub-sections below, to achieve this objective, in one study, in individual mice we profiled ProSense750 radiance in the lungs immediately after a single i.v administration; given either 18 hours or 42 hours after final HDM challenge when inflammation is predominantly neutrophilic or eosinophilic, respectively. After dye injection we continued to measure thorax radiance at 6-hour intervals thereafter. In a second study in individual mice we administered ProSense750 18 hours after final HDM challenge as above, but then also provided a second i.v. administration of dye 24 hours later (42 hours after final HDM challenge). Again, we imaged the thorax immediately after both injections and at 6 hour intervals thereafter for an additional 30 hours. For all the experiments above we also included allergen-naïve mice, and performed ProSense750 administration and optical imaging in a time matched manner to generate control data.

9.3.1 Single Injection – 18 hours post Challenge

Our initial study was performed in mice by administering ProSense750 (100μL of 4nM) 18 hours after the final HDM challenge in our acute (2-week) protocol, and in time-matched allergen naïve mice. Temporal patterns of thoracic radiance from three HDM challenged animals and mean data from this group are shown in **Figure 10A and Figure 10B**.

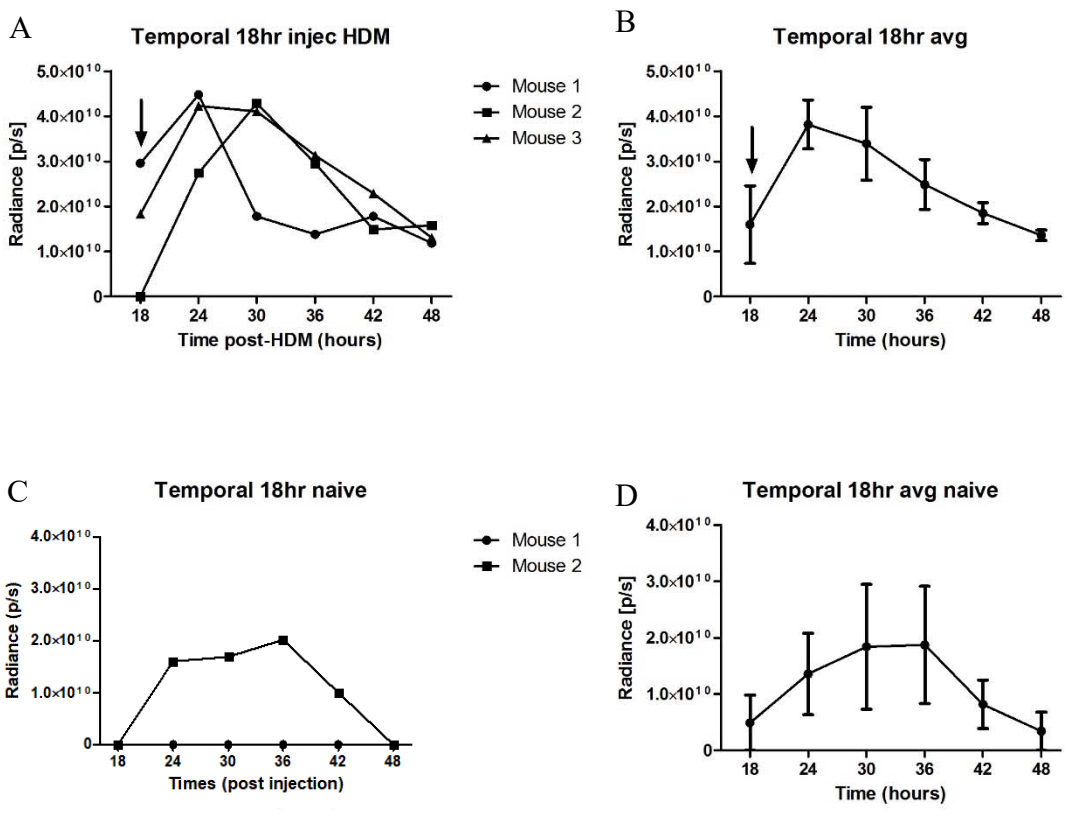

Figure 10: Kinetics of thoracic radiance after ProSense750 administration 18 hours post HDM challenge. Mice underwent a 2-week acute HDM challenge protocol (n=3), or time matched allergen-naive mice (n=2) were used. ProSense750 (100µl, 4nM) was administered 18 hours after the final allergen challenge (indicated by arrow), and a thoracic image was obtained immediately thereafter (within 1 minute)(18 hour time point in each graph), as well as at 6 hour intervals thereafter. IVIS Spectrum image capture settings used were: 1 sec exposure | f/stop = 2 | lamp level low. A) Temporal record of thoracic radiance in individual HDM challenged mice. B) Mean data for thoracic radiance of HDM challenged mice. C) Temporal record of thoracic radiance in individual allergen naïve mice. D) Mean data for thoracic radiance of allergen-naïve mice. Data in panels B and D represent mean ± standard deviation.

Thoracic radiance increased rapidly, reaching a peak 6 hours after ProSense750 administration (corresponding to 24 hours post HDM-challenge). Peak fluorescence was maintained for at least an additional 6 hours (12 hours post dye injection), but declined by ~50% 12 hours after peak radiance was attained (18 hours after dye administration). Twenty-four hours

after ProSense750 administration, thoracic radiance had declined to what we measured immediately after the dye had been injected.

Temporal patterns of thoracic radiance from allergen naïve mice and mean data from this group are shown in **Figure 10C and Figure 10D.** Mean peak radiance was attained from 12-18 hours post injection of ProSense750. However, peak radiance was significantly lower than that we measured in HDM challenged mice. Similar to HDM challenged mice, 24-30 hours after ProSense750 administration, thoracic radiance in allergen naïve mice returned to levels similar to that measured immediately after dye injection.

9.3.2 Single Injection – 42 hours post challenge

We next determined the temporal pattern of a single administration of ProSense750 42 hours after the final HDM challenge in our acute, 2-week allergen exposure protocol. Temporal patterns of thoracic radiance from three HDM challenged animals and mean data from this group are shown in **Figure 11A and Figure 11B**.

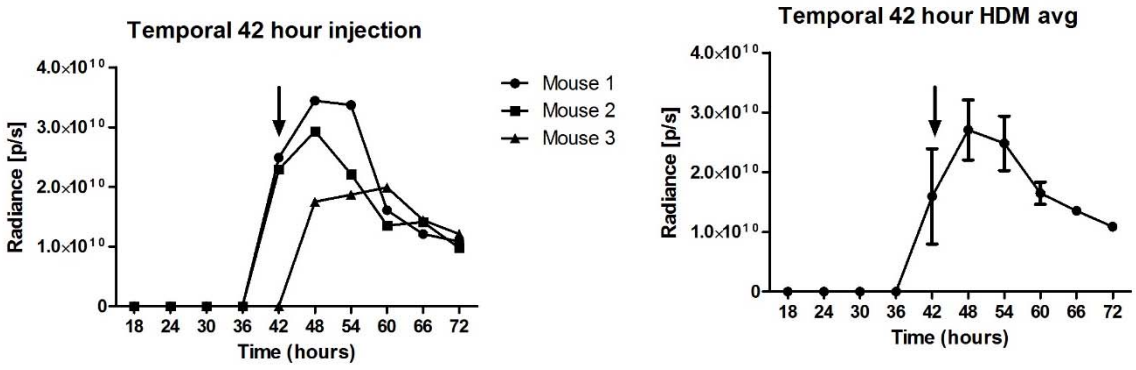

Figure 11: Kinetics of thoracic radiance after ProSense750 administration 42 hours post HDM challenge. Three mice underwent a 2-week acute HDM challenge protocol, then ProSense750 (100µl, 4nM) was administered 42 hours after the final allergen challenge (indicated by arrow), and a thoracic image was obtained immediately thereafter (within 1 minute)(42 hour time point in each graph), as well as at 6 hour intervals thereafter. IVIS Spectrum image capture settings used were: 1.5 sec exposure | f/stop = 2 | lamp level low. A) Temporal record of thoracic radiance in individual HDM challenged mice. B) Mean data for thoracic radiance of HDM challenged mice. Data in panel B represent mean ± standard deviation.

The temporal pattern we observed was similar to what we observed with ProSense750 administered 18 hours post-allergen change. Thoracic radiance increased rapidly, reaching a peak 6 hours after dye injection (corresponding to 48 hours post HDM challenge). Peak fluorescence was maintained for at least an additional 6 hours (12 hours post dye injection), but declined by ~50% 12 hours after peak radiance was attained (18 hours after dye administration). Twenty four hours after ProSense750 administration, thoracic radiance had declined to that we measured immediately after the dye had been injected.

9.3.3 Duel Injection

As our analysis of the kinetics of ProSense750 radiance in the lungs after a single injection revealed that the signal may only be maintained at optimal levels for 6-12 hours, we next performed a study to determine whether the addition of a second, delayed dye injection in the same animal might broaden the window over which measurement of stable lung radiance could be performed. This is important as with the murine HDM challenge model that we employ, there are at least three critical time points that necessitate tracking of lung inflammation: (1) 6-8 hours after final allergen challenge (when inflammation is predominantly neutrophilic, but there is little change in the responsiveness of airways to inhaled methacholine); (2) 24 hours after final allergen challenge (when inflammation is predominantly eosinophilic, but only mild-to-moderate changes in airway responsiveness to inhaled methacholine are evident); and, (3) 48 hours after final allergen challenge (when inflammation is predominantly eosinophilic, and airway hyperresponsiveness to inhaled methacholine is significant).

For this quality control study we used three mice that had been subjected to our 2-week HDM challenge protocol and performed repeated IVIS optical imaging every 6 hours for 54 hours, beginning 18 hours after final allergen exposure with an initial tail vein administration of ProSense750 (100μL, 4nM). Each mouse received a similar second i.v. ProSense750 administration 24 hours later (42 hours after final allergen exposure), and sequential imaging was continued for an addition 30 hours, reaching 72 hours post final allergen exposure **(Figure 12)**.

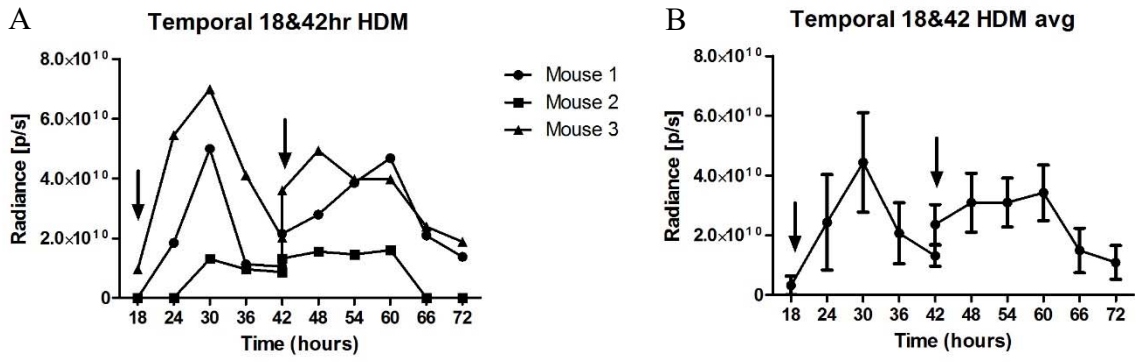

Figure 12: Kinetics of thoracic radiance after dual injection of ProSense750: 18 and 42 hours post HDM challenge. Three mice underwent a 2-week acute HDM challenge protocol, then ProSense750 (100µl, 4nM) was administered 18 hours after the final allergen challenge (indicated by first arrow). A thoracic image was obtained immediately thereafter (within 1 minute)(18 hour time point in each graph), as well as at 6 hour intervals thereafter. At 42 hours post allergen challenge a second i.v. administration of ProSense750 (100µl, 4nM) was given to each animal (indicated by an arrow). A thoracic image was obtained immediately thereafter (within 1 minute)(42 hour time point in each graph), as well as at 6 hour intervals for an additional 30 hours. IVIS Spectrum image capture settings used were: 1.25 second exposure | f/stop = 2 | lamp level low. A) Temporal record of thoracic radiance in individual HDM challenged mice. B) Mean data for thoracic radiance of HDM challenged mice. Data in panel B represent mean ± standard deviation.

As we observed in prior experiments, injection of ProSense750 18 hours after allergen challenge resulted in a gradual rise to peak thoracic radiance 6 hours later that was sustained for an additional 6 hours. The second administration of ProSense750, 42 hours after allergen challenge, almost immediately restored peak thoracic radiance, and peak radiance was sustained for an additional 18 hours before returning to a level comparable to that measured immediately after the first dye administration (18 hours after allergen exposure). Thus, though a second administration of ProSense750 did not generate higher lung radiance than we measured after a single injection, the time to reach peak radiance was markedly faster ("immediate" vs 6 hours), and more sustained (18 hours vs. 6 hours) than is attained with only a single administration of the cathepsin-activated fluorescent agent.

9.4 Effects of Simvastatin and Fluticasone Propionate on ProSense750 Lung Radiance

To determine whether optical imaging of ProSense750 of the lungs in HDM challenged mice is sufficient to discern the inhibitory effects of anti-inflammatory therapy we next used IVIS optic imaging technology to compare thoracic radiance in mice treated with intra-nasally instilled glucocorticoid or simvastatin. Mice were subjected to our 2-week HDM challenge protocol, and received either daily allergen alone, or daily allergen with simvastatin (31.25 ng (1.6μg.kg); 62.5ng (3.1μg/kg); or 125ng (6.25μg/kg)), or fluticasone propionate (10μg/kg). We performed whole body imaging on 6 mice in each group to measure ProSense750 lung radiance.

Whole body imaging revealed that intranasal simvastatin significantly reduced cathepsin-activated ProSense750 lung radiance induced by repeated challenge with HDM (One way ANOVA, N=3, p=0.04)**(Figure 13A and Figure 13B)**.

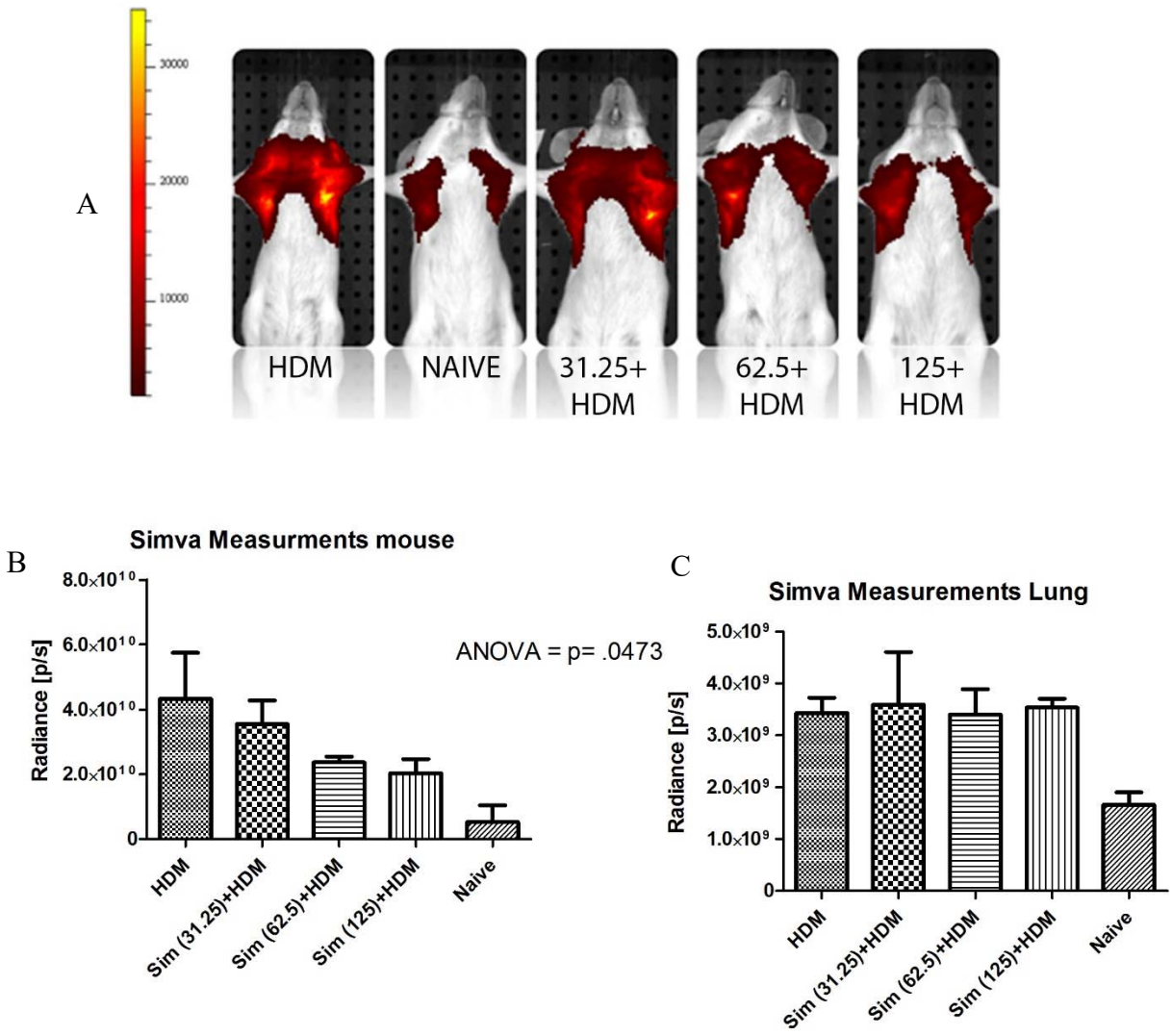

Figure 13: Effects of intranasal simvastatin therapy on cathepsin-activated ProSense750 lung radiance in HDM challenged mice. Mice underwent a 2-week acute HDM challenge protocol **(HDM)**, or were simultaneously co-treated with intranasal simvastatin **(Sim)** (31.25ng (1.6µg.kg); 62.5ng (3.1µg/kg); or 125ng (6.25µg/kg)). ProSense750 (100µl, 4nM) was administered 18 hours after the final allergen challenge and optical imaging with the IVIS Spectrum was performed 6 hours later. Allergen-naïve **(Naïve)** mice were used as time-matched controls. (A) Typical whole body images, corrected for baseline radiance, showing chest radiance in Naïve, HDM challenged, HDM-simvastatin treated mice using image capture settings of: 0.75 second exposure | f/stop = 2 | lamp level low. (B) Mean data for thoracic radiance in whole animal imaging for each group (N=3) (*$p<0.05$, compared to HDM-only mice, One Way ANOVA). (C) Mean data for ProSense750 radiance measured in excised lungs from animals in each group. IVIS Spectrum image capture settings were 0.75 second exposure | f/stop = 2 | lamp level low. (N=3)(*$p<0.05$, compared to HDM-only mice, One Way ANOVA). Data in panels B and C represent mean ± standard deviation.

Simvastatin concentration-dependent reduction in ProSense750 lung radiance was evident; however, non-parametric post hoc analysis (Bonferroni correction) did not confirm statistical difference between groups treated with different concentrations of simvastatin

Whole body imaging of HDM-challenged mice that were treated with intranasal fluticasone propionate to blunt inflammation revealed that, in contrast to the effects of repeated intra-nasal instillation of simvastatin (125ng), glucocorticoid intervention had no impact on ProSense750 chest radiance **(Figure 14A)** (One Way ANOVA, N=3, $p>0.05$).

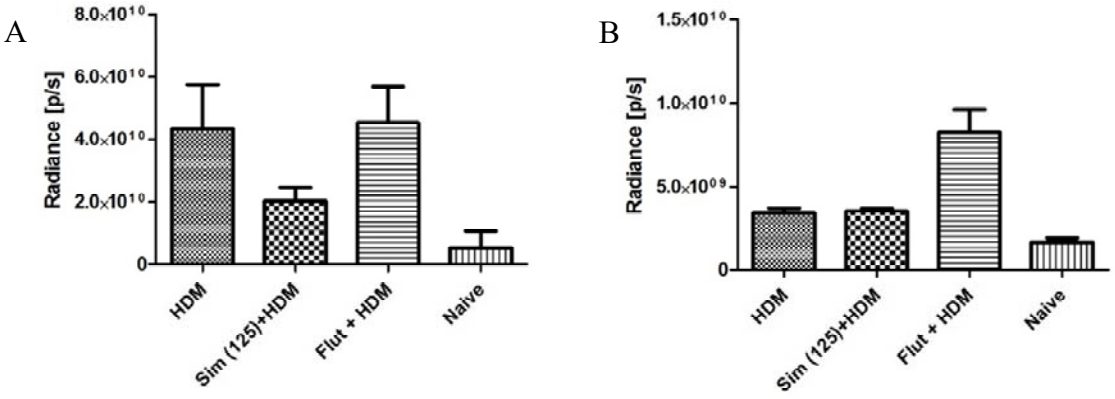

Figure 14: Effects of intranasal fluticasone propionate and simvastatin therapy on cathepsin-activated ProSense750 lung radiance in HDM challenged mice. Mice underwent a 2-week acute HDM challenge protocol **(HDM)**, or were simultaneously co-treated with intranasal simvastatin **(Sim)** (125ng (6.25µg/kg)) or fluticasone propionate **(Flut)**(10µg/kg). ProSense750 (volume and concentration in nM) was administered 18 hours after the final allergen challenge and optical imaging with the IVIS Spectrum was performed 6 hours later. Allergen-naïve **(Naïve)** mice were used as time-matched controls. (A) Mean data for thoracic radiance in whole animal imaging for Naïve, HDM challenged, HDM-simvastatin and HDM-Flut treated mice. IVIS Spectrum image capture settings were 0.75 second exposure | f/stop = 2 | lamp level low. (B) (N=3) (*$p<0.05$, compared to HDM-only mice, One Way ANOVA, with Bonferroni post hoc analysis). (B) Mean data for ProSense750 radiance measured in excised lungs from animals in each group. IVIS Spectrum image capture settings were 0.75 second exposure | f/stop = 2 | lamp level low. (N=3)(*$p<0.05$, compared to HDM-only mice, One Way ANOVA). Data are shown as mean ± standard deviation.

This suggests that fluticasone propionate therapy was not sufficient to prevent allergen challenge-associated activation of cathepsins in the lung. Furthermore, additional imaging of excised lungs revealed significantly greater ProSense750 radiance in specimens from fluticasone propionate treated, HDM-challenged mice, than those from mice receiving 2-week HDM challenge alone, or simultaneous HDM challenge and intranasal simvastatin (One Way ANOVA, with Bonferroni correction, N=3, $p<0.05$)**(Figure 14B).**

9.5 Effects of Allergen Avoidance on ProSense750 Radiance in Lungs

We next tested the capacity to use in vivo optical imaging of ProSense750 radiance to track effects of a non-pharmacological intervention (allergen avoidance) to reverse established allergic lung inflammation in mice. For this study, mice were subjected to our 2-week HDM challenge protocol then were maintained without further allergen challenge for up to an additional 2 weeks to mimic an allergen avoidance intervention. Mice in this study were assessed 48 hours after allergen challenge when maximum inflammation is present, as well as 1 week or 2 weeks post-HDM challenge using: whole body optical imaging for ProSense750 radiance using the IVIS Spectrum instrument to assess cathepsin-associated inflammation; and, bronchoalveolar lavage to collect, count and perform immune cell differential analysis to assess whole lung inflammation. As expected lung ProSense750 radiance was markedly elevated after 2 weeks repeated allergen challenge (48 hour avoidance group) compared to that measured in our previous studies using allergen naive mice. However, interestingly, in vivo imaging did not reveal any significant loss of thoracic ProSense750 radiance over the 2 week duration of allergen avoidance thereafter **(Figure 15)**.

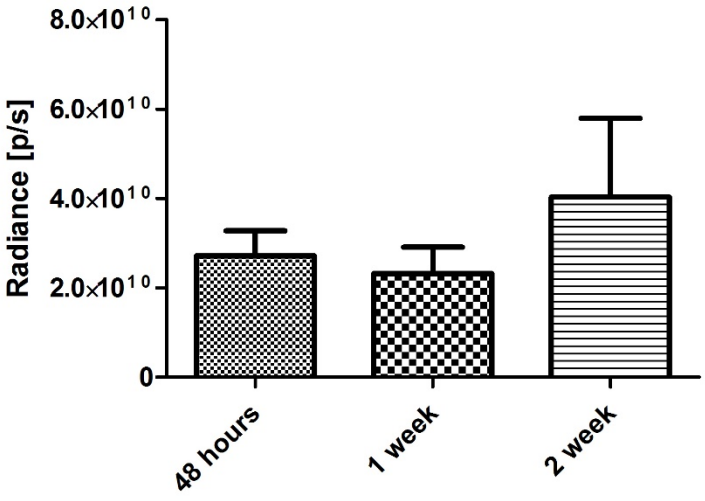

Figure 15: Effects allergen avoidance on ProSense750 lung radiance in mice with established allergic lung inflammation. Mice underwent a 2-week acute HDM challenge protocol then were maintained for an additional 48 hours, 1 week or 2 weeks without allergen challenge. At each time point, ProSense750 (100µl, 4nM) was administered 6 hours before optical imaging with the IVIS Spectrum, with instrument setting: *1.5 second exposure |f/stop = 2 | lamp level low*. Mean data for thoracic radiance in whole animal imaging was determined from that measured in 3 different animals at each time point. Data are shown as mean ± standard deviation. No statistically significant difference was evident between different duration allergen avoidance groups ($p>0.05$ compared to 48 hours avoidance group, One Way ANOVA.

In fact, thoracic ProSense750 appeared to increase somewhat after 2 weeks of allergen avoidance, but this was not statistically significant compared to radiance measured 48 hours or 1 week post-HDM challenge (One Way ANOVA, N=3 for each group, $p>0.05$).

We next assessed the correlation between cathepsin-activated ProSense750 lung radiance with an independent index of lung inflammation, immune cell counts in lung lavage, using animals subjected to our allergen avoidance protocol **(Figure 16)**.

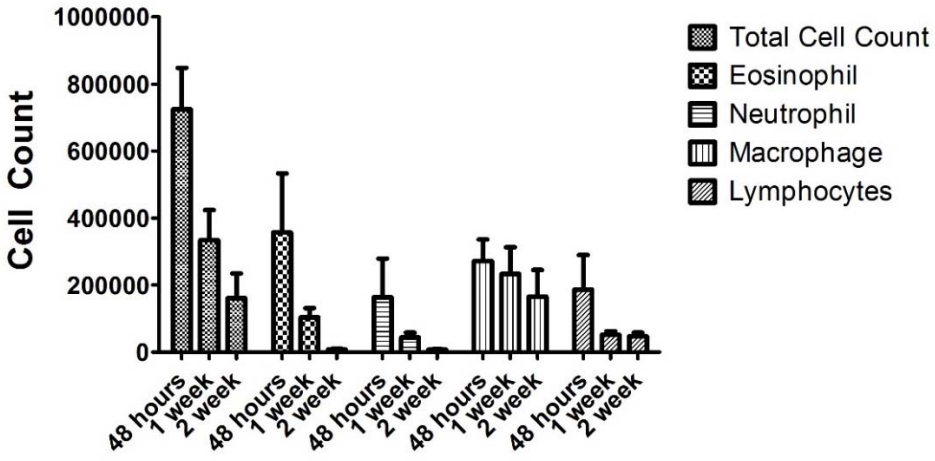

Figure 16: Immune cell counts in bronchoalveolar lavage collected from 2-week HDM challenged mice then subjected to allergen avoidance. Mice underwent a 2-week acute HDM challenge protocol then were maintained for an additional 48 hours, 1 week or 2 weeks without allergen challenge. At each time point bronchoalveolar lavage was performed and subsequent cell counting and differential analysis completed. Mean data for cell counts in 3 different animals at each time point are shown ± standard deviation. Total and individual cell counts decreased significantly in a disparate manner with duration of allergen avoidance (N=3 for each group; One way ANOVA with Bonferroni post hoc analysis, *$p<0.05$ compared to 48 hour avoidance group)

Maximum number of cells – total and individual immune cell types – was attained 48 hours after ceasing allergen challenge, which is consistent with our published data using the 2-week HDM protocol [97]. We observed a significant decrease in the total number of lung lavage immune cells after one week and this decreased further, almost to numbers similar to allergen-naïve animals (not shown) after two weeks of allergen avoidance (N=3 for each group, One Way ANOVA, $p<0.05$ compared to 48 hours post allergen challenge). This pattern was mirrored for eosinophils, neutrophils and macrophages, whereas lymphocyte number rapidly decreased to levels near that of allergen-naive animals within one week, therefore remained the same after two weeks allergen avoidance.

9.5.1 Correlation of lung lavage cell number with ProSense750 lung radiance

In our allergen avoidance experiment we collected ProSense750 optical imaging day and performed bronchoalveolar lavage for cell counting and differential analysis on each animal at each allergen avoidance time point. Thus, we pooled all data (irrespective of avoidance duration) to assess the correlation between cell counts in individual mice **(Figure 17).**

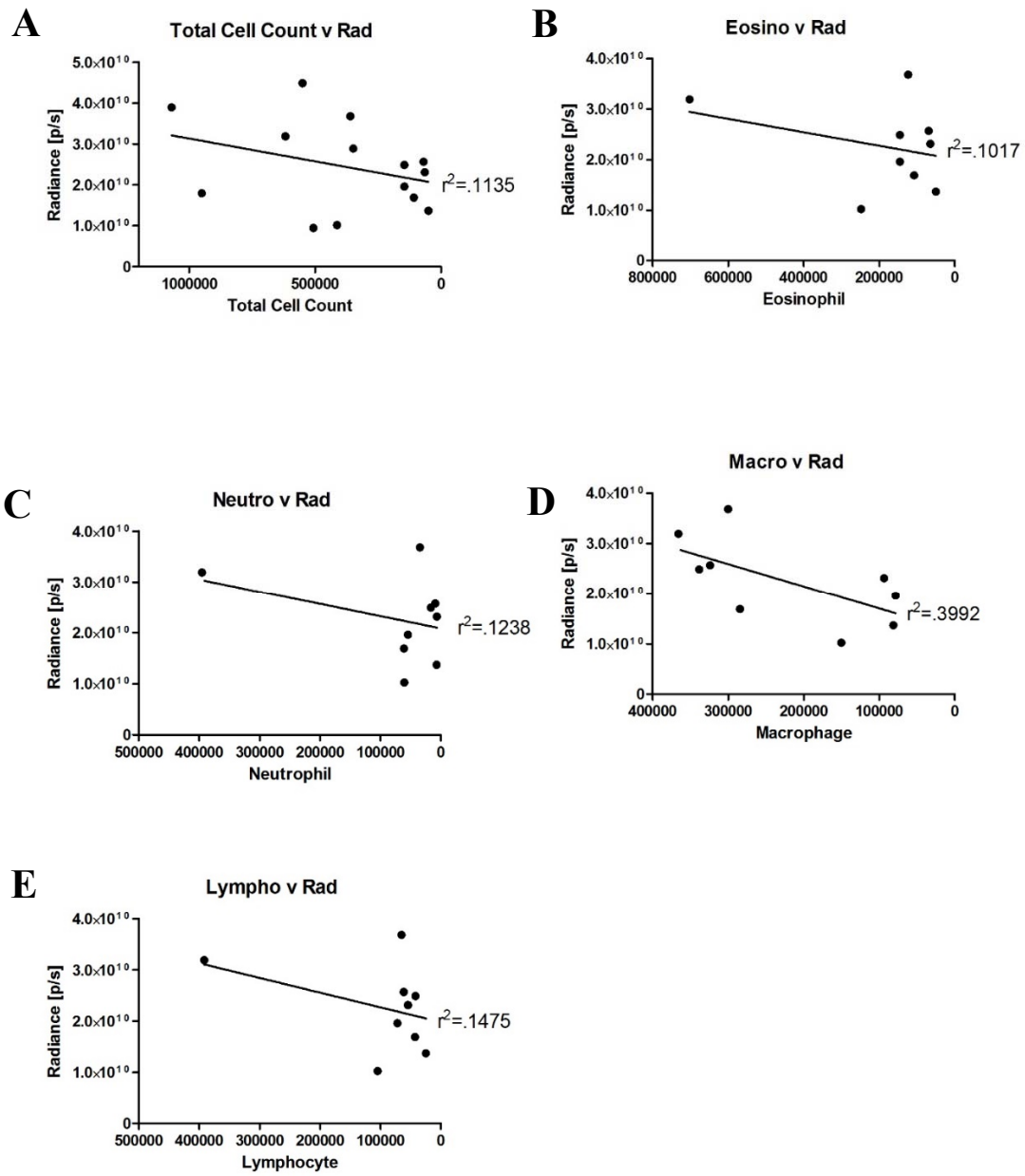

Figure 17: Correlation between lung lavage immune cell number and ProSense750 lung radiance in individual mice after HDM challenge and allergen avoidance. Mice underwent a 2-week acute HDM challenge protocol then were maintained for an additional 48 hours, 1 week or 2 weeks without allergen challenge. At each time point, mice in each group (N=3) underwent IVIS Spectrum optical imaging for ProSense750 as described for Figure 15. After imaging bronchoalveolar lavage was performed and subsequent cell counting and differential analysis completed. Panels A (N=14) and B-E (N=9) show plots of matching data from mice in all groups. Linear correlative analysis to determine r^2 correlation between ProSense750 radiance and total and individual immune cell number (shown in each panel).

When data from individual mice were plotted we did not observe any significant correlation between thoracic ProSense750 radiance and total or different immune cell counts, as no correlation coefficient, $r^{2,}$ was determined to be greater than 0.95, as indicated in **Figure 17A-E**. To account for the significant variability in cell counts and radiance we observed between animals, we next pooled the data for the 3 mice in each allergen avoidance group, and plotted mean values for radiance and total or individual immune cell counts to assess the degree of correlation between optical imaging measurement of cathepsin activity-associated lung inflammation and that indicated by immune cell number in lung lavage **(Figure 18)**

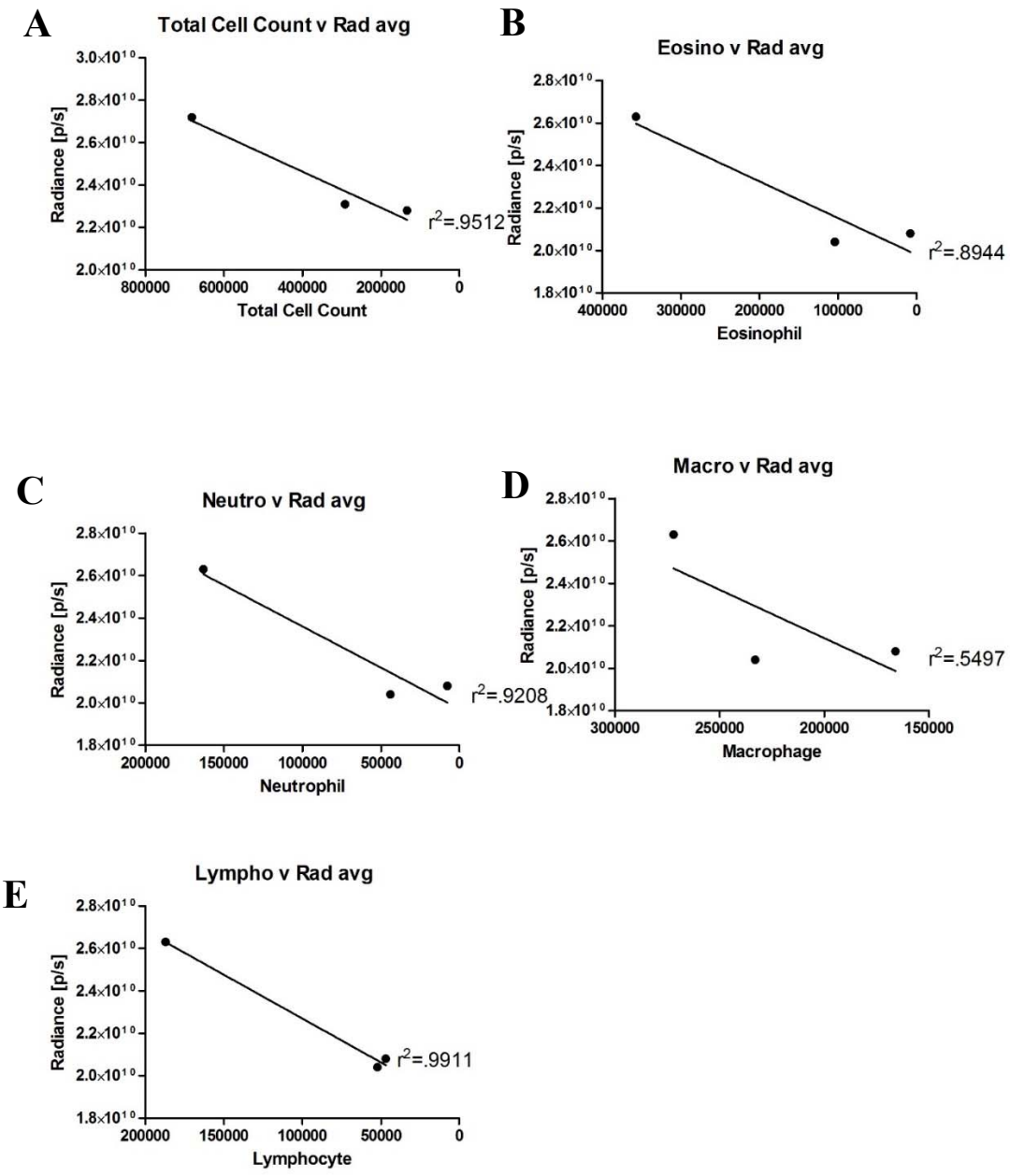

Figure 18: Correlation between lung lavage immune cell number and ProSense750 lung radiance in different duration allergen avoidance groups after HDM challenge. Mice underwent a 2-week acute HDM challenge protocol then were maintained for an additional 48 hours, 1 week or 2 weeks without allergen challenge. At each time point, mice in each group (N=3) underwent IVIS Spectrum optical imaging for ProSense750 as described for Figure 17. After imaging bronchoalveolar lavage was performed and subsequent cell counting and differential analysis completed. Panels A-E show plots of matched mean data for each group. Linear correlative analysis was performed to determine r^2 correlation between ProSense750 radiance and total and individual immune cell number (shown in each panel). Correlation was considered statistically significant if r^2 was >0.95.

Interestingly, using this approach the r^2 correlation coefficient between ProSense750 lung radiance with either total cell count (r^2= 0.95), neutrophil number (r^2 = 0.92), and lymphocyte number (r^2 = 0.99) was significant. Conversely, though the r^2 correlation for lung eosinophil (r^2 = 0.89) and macrophage number (r^2 = 0.55) was markedly enhanced compared to individual animal analyses, statistical significance was not reached.

9.6 Induction of autophagy by pro-inflammatory cytokines: human airway smooth muscle cells

A goal of this project is to use in vivo imaging to measure effects of potential asthma therapies on allergic lung inflammation in mice using a pre-clinical experimental design. Autophagy is emerging as a modulator of inflammation and tissue repair in a number of disease states, including human asthma [79-81]. Prior to launching a study investigating the impact on an autophagy inhibitor, chloroquine, on lung inflammation in HDM challenged mice we aimed to establish whether inflammation induced autophagy in lung cells. For this purpose we used primary cultured human airway smooth muscles cells, and used immunoblotting to measure whether the abundance of protein biomarkers of autophagy was affected by exposure to a cocktail ("cytomix") of asthma-associated cytokines: INFγ, IL-β and TNFα**.** We used Western blotting to track the temporal pattern of abundance of LC3-II, a marker of autophagosome accumulation, from 0-96 hours of "cytomix" exposure **(Figure 19)**. Accumulation of LC3-II and a concomitant relative increase in the ratio of LC3-II:LC3-I was evident in each cell line investigated, and was on par with LC3-II accumulation in response to the autophagy inducer, rapamycin (48 hours).

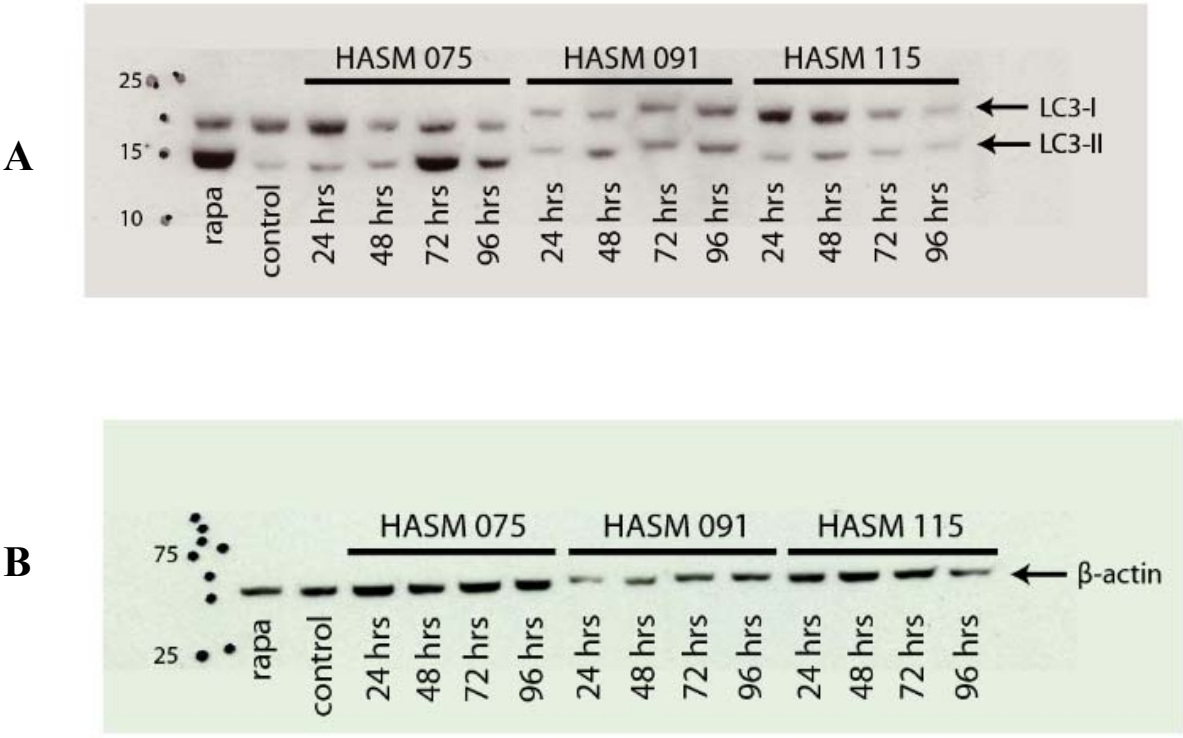

Figure 19: Immunoblot analysis of the effects of "cytomix" exposure on autophagy marker abundance in human airway smooth muscle cells. As detailed in Methods, three low passage number cell cultures (HASM075, HASM091, and HASM115) were grown to confluence, maintained in serum free conditions for 24hrs then treated with "cytomix" (10ng/mL of IFNγ, IL-1β and TNFα) for up to 96 hours prior to obtaining total protein lysates. For negative controls, protein lysates were harvested to serum-free culture, and for a positive control lysates were obtained from cultures treated with the autophagy inducer, rapamycin (**rapa**)(1μg/mL) for 48 hrs prior to preparing protein lysates for immunoblotting, using 10μg total protein load per gel ane.. (A) Typical immunoblot for autophagy marker, LC3-II. LC3-I is also shown, an increase in LC3-II/LC3-I ratio is indicative of autophagy. (B) Immunoblot for loading control β-actin for immunoblot shown in panel A.

9.7 Effect of autophagy inhibitor, chloroquine, on allergic asthma inflammation

Chloroquine (CQ), inhibits autophagolysosme and lysosome function, thus is a suppressor of autophagy that has been tested for its therapeutic effects in a number of cancer-related preclinical studies [162, 163]. Given our *in vitro* evidence that asthma cytokines can

induce autophagy in lung cells, we next used *in vivo* optical imaging to measure the effects of intraperitoneally injected CQ (10μL, 50 mg/mL) on lung inflammation. We delivered CQ to mice in a prevention protocol, administering it prior to individual intranasal HDM challenges over the course of our standard 2-week protocol. For control mice we also administered CQ in allergen-naive mice. Optical imaging for ProSense750 radiance in the thorax was performed 48 hours post HDM challenge. After imaging we also performed broncholaveolar lavage to collect immune cells for counting and differential analysis. Though a there appeared to be a trend for increased ProSense750 thoracic radiance in animals treated with chloroquine, the *in vivo* ProSense750 signal was variable and CQ treatment did not have a statistically significant effect on lung fluorescence induced by HDM challenge (**Figure 20**) (N=2, One Way ANOVA, P=0.49).

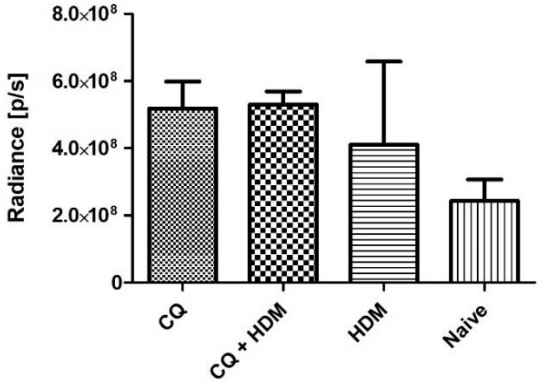

Figure 20: Effects of chloroquine (CQ) on ProSense750 lung radiance in HDM challenged and allergen-naïve mice. Mice underwent either a standard 2-week acute HDM challenge protocol (HDM), or were also co-treated with an intraperitoneal CQ injection (50 mg/kg) prior to each HDM challenge (CQ + HDM). As controls, allergen-naïve mice with (CQ) or without CQ (Naïve) therapy were also studied. 2 animals were included in each group. ProSense750 (100μl, 4 nM) was administered 6 hours before optical imaging with the IVIS Spectrum, performed 48 hours after final allergen challenge (instrument settings: *1.0 second exposure |f/stop = 2 | lamp level low)*. Mean data for thoracic radiance in whole animal imaging was determined from that measured in 2 different animals. Data are shown as mean ± standard deviation. No statistically significant difference was evident between different duration allergen avoidance groups (P=0.49, One Way ANOVA.

We also assessed total and differential cell counts in bronchoalveolar lavage to determine whether the effects of CQ on ProSense750 radiance reflected its therapeutic impact on inflammatory cell influx to the lung **(Figure 21).**

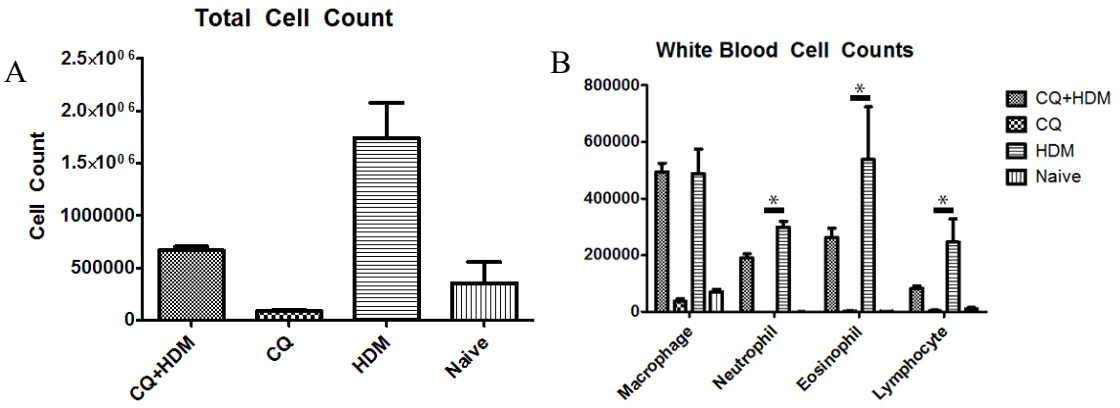

Figure 21: Effects of chloroquine (CQ) on immune cell influx in HDM challenged and allergen-naïve mice. Mice underwent either a standard 2-week HDM challenge protocol (HDM), or were also co-treated with an intraperitoneal CQ injection (50 mg/kg) prior to each HDM challenge (CQ + HDM). As controls, allergen-naïve mice with (CQ) or without CQ (Naïve) therapy were also studied. 3 animals were included in each group. Bronchoalveolar lavage was collected after optical imaging, 48 hours after final allergen challenge and cell counting and differential analysis completed. Mean data ± standard deviation for cell counts in 3 different animals in each group are shown. (A) Total cell count was significantly higher in HDM challenged animals compared to CQ+HDM, Naïve and CQ-only mice (One Way ANOVA with post hoc Bonferroni correction, *P<0.05). Total immune cell number in CQ+HDM was significantly higher than in Naïve of CQ animals (One Way ANOVA with post hoc Bonferroni correction, #P<0.05). (B) CQ treatment significantly reduced the number of eosinophils, lymphocytes and neutrophils in the lungs of HDM-challenged mice (One Way ANOVA with post hoc Bonferroni correction, *P<0.05), but had no effect on HDM challenge associated lung macrophage number (One Way ANOVA, n.s., P>0.05).

In contrast to its effects on lung ProSense750 radiance, CQ significantly inhibited HDM challenged-induced total lung immune cell accumulation by nearly 60% **(Figure 21A)**(N= 3; One Way ANOVA with post hoc Bonferroni correction, P<0.05). Despite its inhibitory effects

on immune cell influx, total immune cell number in HDM challenged mice treated with CQ remained higher than in allergen-naïve or CQ treated allergen-naïve animals (One Way ANOVA with post hoc Bonferroni correction, $P<0.05$). CQ alone had no significant effects on immune cell number in the lungs of allergen-naïve mice.

Among individual immune cell types **(Figure 21B)**, CQ treatment inhibited eosinophil and macrophage accumulation in HDM challenged animals by more than 50% and 60%, respectively (N= 3; One Way ANOVA with post hoc Bonferroni correction, P=*<.05). HDM-induced neutrophil influx to the lungs was blunted by ~30% by CQ treatment (N= 3; One Way ANOVA with post hoc Bonferroni correction, P=<.05), however, it did not affect macrophage number in the lungs (N= 3; One Way ANOVA with post hoc Bonferroni correction, $P>0.05$).

10. DISCUSSION

The research described in this thesis aligns with a research direction that recognizes a need to decipher pathophysiologic processes that are associated with asthma in small animal models, enabling pre-clinical testing, but requiring novel technologies that support repeated measurements over time to track processes and responses in individual animals [164]. Innovation of this nature can underpin new and unexpected insight, as well as promoting cost and time efficiencies by customizing research programs to identify complementary markers of disease [165]. More traditional experimental procedures provide an established 'gold standard' to confirm whether newer more efficient approaches are valid and reliable. As presented we have done a quality control study for a new procedure by using established models and technologies in combination with one another to provide more robust insight into disease pathophysiology. Non-invasive imaging, as a newer innovation that is becoming more accessible to researchers in general is moving to the forefront of basic science research, providing real-time *in vivo* and *ex vivo* insight about disease process and response to emerging therapies.

10.1 Non-invasive Imaging

Non-invasive *in vivo* imaging provides an alternative quantitative procedure to more invasive or traditional techniques. Depending on which imaging modality is being used, different measurements and conclusions associated with disease pathophysiology and biology can be obtained. For many years, non-invasive imaging provided capacity to perform anatomical scans to assess structural change in organs of interest in disease states such as cardiomyopathy [166]. With medical imaging technology improvements, capacity to measure physiological function as well as to detect changes with more resolution in smaller organs or regions of organs has

emerged. As we have done in the work for this thesis, this technology is not routinely applied for animal research. Ultrasound and MRI has been used for a majority of studies, but other imaging modalities, including optical imaging, has become a far more cost effective and multi-functional alternative in today's research climate [167].

Optical imaging uses the properties of light in conjunction to unique disease molecules and photography to generate an image which can be used to create a measureable value [155]. A sub-modality of optical imaging is fluorescent imaging that uses a reporter molecule with defined excitation and emission characteristics, and that can be activating by a biological process or targeted to s specific organ or cell type [168]. The aim of this thesis was to generate a working protocol to measure the inflammatory response in the lung associated with a murine allergen-challenge mode of asthma.

10.2 Autofluorescence determination

All biological tissues *in vivo* emit autofluorescence that can decrease the signal-to-noise ratio in fluorescence optical imaging, thereby potentially masking real biological signals or creating false positive signal. To compensate for autofluorescence *in vivo,* common practice is to collect a baseline fluorescent signal from the study animal or from a treatment-matched control, and use this to discriminate signal from background signal [111, 140] Using software algorithms, baseline autofluorescence signal is subtracted from the signal measured for a fluorescent probe. Working *in vivo*, this is complicated somewhat by the fact that source of autofluorescence may be generated by several different structures and organs. As an example, in a pilot experiment for my work I performed a spectral un-mixing correction using operational and analytic software of the IVIS Spectrum Optical Imager in an effort to isolate the sources of

autofluorescence in control (allergen-naïve) mice. In mice fed regular chow *ad libitum* that contains alfalfa, we detected autofluorescence signals $1x10^{10}$p/s in the lungs, skin, and most prominently, the intestinal tract. While the signals from the rest of the body were minimal, the intensity and character of the auto-signal from the intestinal tract had the potential to generate an additional signal that overlaps the thoracic region. Thus, throughout our studies we routinely collected autofluorescence background and with IVIS Spectrum software corrected measurements of ProSense750 radiance in the thorax. Notably, consistent with prior published reports [139], the primary source of autofluorescence appears to be the food ingested by the mice. Since regular mouse chow contains significant, if not variable amounts of alfalfa and as such is an enriched source for chlorophyll, it has broad excitation and emission spectra that underpin a significant capacity for fluorescence [139]. For this reason, for all of our studies mice were placed on an alfalfa-free diet to dampen food-associated autofluorescence and minimize perturbation of optical imaging for ProSense750 (**Figure 7**). Using an alfalfa-free diet also aligned our protocols with previously published studies that also ensured the intestinal autofluorescence signals did not interfere with lung radiance [169].

10.3 Imaging Parameters

For experimentation, optimization of optical imaging was essential, thus we performed a number of quality control studies to establish baseline parameters for obtaining images. The IVIS Spectrum imager enables capacity to modify a number of parameters for image capture, including f-stop, pixel binning, exposure time and lamp level. In order for an image to be captured reliably the number of excited photons hitting the light sensor (counts as per IVIS system) needs to be between 600 and 60 000, thus image capture parameters need to be adjusted

to be within the threshold. For each set of mice in each study, the same imaging parameters were used. Another imaging issue to consider was the complexity of imaging the signal from an internal organ in an intact, freely breathing animal, hence multiple tissues and could mask or perturb the radiance of interest and this might be affected by breathing or heart movement. To overcome this issue we routinely captured 20 images from each animal over a 20 second interval to allow for variation in inflammation signal, variability in the size of the animal and effects of different chest position due to breathing. Using this catalogue of images, the same parameters could be used during the post processing and normalization of image signals for reproducible quantification in different mice, studied at different times.

10.3.1 Dye concentration

The first parameter which was modified to determine an optimal optical imaging protocol was the amount of ProSense750 injected into reach animal. Starting with the manufacturer's guidelines, 100µL of 4nmol ProSense750, we investigated the effects of decreasing the dye load 2nmol, 1nmol and 0.5nmol in both HDM-challenged and -naïve mice. Epi-illumination analysis revealed that a signal could only be readily detected at the suggested concentration, thus for our work the manufacturer's guidelines were used to allow for the greatest flexibility in optimizing image acquisition parameters.

10.3.2 Imaging exposure values

Noninvasive *in vivo* imaging has numerous variables that can contribute to the overall image and signal quality and contribute to that variability [111]. These can vary depending on the model being used, thus from the murine anatomical standpoint; size, tissue depth, and signal

strength can vary uniquely [170]. As noted above, the IVIS Spectrum has the capacity to modify the exposure time, f/stop, lamp level, and image binning. For each animal we obtained multiple images using different capture parameters to ensure reliable comparison of images between animals on a given day, and well as between animals studied on different days. This approach has been previously highlighted as being a critical needed component for optical imaging protocols [170]. Thus, for each set of images we included a range of parameters to ensure optimal radiance count threshold - above minimum detection and below saturation - was used. Using this approach, the same parameter settings could be used for different experiments in this thesis.

10.3.3 Injection Quality

Perhaps the most important direct technical determinant of ProSense750 thoracic radiance was the injection quality of the tracer agent. The diameter of a mouse tail vein is approximately equivalent to a 30 gauge needle. At this small size, even the most skilled technician's hands cannot deliver dye by tail vein injection without some variability. If the vein is compromised during injection, or the needle not fully entered there is significant potential for dye to by-pass the systemic circulation and collect in the perivascular space near the injection site. This would reduce the amount of tracer that is disbursed to the lung for eventual activation, thus contributing to an artefactual muting of measurable ProSense750 radiance. To account for this source of variability we developed an injection quality scoring system and compared the injection quality to the measured thoracic radiance. For this purpose we took advantage of the fact that ProSense750 becomes activated almost immediately after injection as cathepsins, the activating agent of the dye, are present at the injection site. This creates an easily detectable

signal that directly reflects the degree of "dye leak", which is inversely proportional to the amount of injected dye that enters the systemic circulation and end organs.

We compared immediate thoracic radiance and that recorded 6 hours after injection with the injection quality in individual animals. Interestingly, if a measurement of thoracic radiance is taken directly after tail vein injection, then there is a correlation with injection quality: chest radiance lower with ineffective injections. As the resting heart rate of a mouse is approximately 700 beats per minute, it takes only a few seconds for the dye to become systematic, thus if less dye is injected into the vascular system, this is rapidly translated to the lungs, with less dye available for activation. A contributing factor to our ability to rapidly detect ProSense750 signal in the lung may be that circulating present in the circulatory system can activate the tracer. Six hours after injection, injection quality had no impact on measurable chest radiance; this is likely due to absorption and slow entry of dye to the circulation over the 6 hour period. Another factor that might be mitigating effects of ineffective tail vein injection on ProSense750 chest radiance 6 hours later is that we used a relatively high abundance of dye that enabled a saturating concentration to reach the lung even if some dye was lost to perivascular leakage. Overall, with 4nM injection, we determined that with a 6 hour injection delay we can reproducibly measure thoracic radiance in the optimal range of the IVIS Spectrum in both allergen-naïve and HDM-challenged mice.

10.4 Kinetics of ProSense750

Via tail vein injection, for cleavage-activated dyes there is a temporal delay in reaching equilibrium in end organs, both the concentration of total dye that accumulates and the stable fraction that becomes activated by a local trigger (eg. cathepsin activity for ProSense750). There

are a number of studies that have examined the kinetics and activities of various proteases, including cathepsins [41, 42, 50-53, 109, 171-175]. We performed quality control experiments to establish when peak activation would occur in mouse injected ProSense750, and to assess how long this signal was maintained before dye quenching of bio-availability began to fall. According to the protocol provided by the manufacturer, imaging was predicted to be optimal and stable 6-24 hours after tail vein injection. Though we found this to be accurate with respect to time to peak lung radiance (6 hours), our data suggest that the peak thoracic signal for a single injection of the dye is only stable for 6 hours. Though our data suggest good correlation of ProSense750 thoracic radiance with lung inflammatory cell counts, the kinetic limitations of studying thoracic radiance outside of a window 6-12 hours pots injection need to be considered, in particular in models where immune cell flux may be significant during and beyond this window of time [26, 48, 91, 176]. Though the scope of our studies did not enable us to elucidate the precise mechanism for loss of dye radiance in the thorax, it seems likely this may be due to loss of bioavailability due to turn over of activated dye, loss of a sufficient pool of inactive (uncleaved) dye to sustain the equilibrium between cathepsin activity and dye turnover, and natural quenching of the fluorochrome.

In additional studies we tracked thoracic radiance in individual mice for up to 72 hours in both allergen-naïve and HDM-challenged mice. We recognized that imaging at multiple time points after allergen challenge was necessary, and our lab's work and that of others show that though inflammation is maximal 24-48 hours after allergen challenge, asthma-like lung dysfunction occurs 48 hours after repeated allergen challenge [97, 159]. For these studies, using insight from our pilot quality control studies, we injected ProSense750 six hours prior to imaging. Though we were able to detect a strong and reliable signal at both 24 hours and 48

hours after allergen challenge, with a single injection peak thoracic radiance could only be measured between 6 and 12 hours posy ProSense750 administration. This suggests that a single injection is suitable for a single or minimally separated timed measurements; however for experiments requiring multiple measurements that are more than 12 hours apart, a second administration of dye is necessary. We performed such a study and our results suggest that with a second administration of dye, an almost immediate return to peak lung radiance was attained and the time for which this was sustained was more than double that we observed with a single dye administration in the same animal. Collectively, these data provide critical insight needed to develop experimental protocols for future long term pre-clinical studies. Though the loss of dye signal is a limitation for the use of optical imaging as presented in his work, it may be possible to develop algorithms to take into account the half-life of the dye in future, and enable normalization that prolongs the reliable window for measuring ProSense750 radiance in the lungs.

10.5 Full Mouse Imaging

The main aim of this project was to determine if the ProSense750 could be used to measure differences in lung inflammation between allergen-naïve and HDM-challenged mice in a manner that reflects established indices of allergic inflammation (ie. immune cell count in the lungs). We acquired thoracic images using trans-illumination mode as using the epi-illumination modality did not allow us to discriminate lung-specific radiance due to significant image capture distortion and interference by the rib cage and signals from other tissues, in particular the bladder and intestinal tract. Using trans-illumination allowed the excitation light signal to be more

directed on and much closer to the lungs, thus isolating the region and reducing diffraction of excitation light.

10.5 Effects of Allergen Avoidance on Lung Inflammation and ProSense750 Thoracic Radiance

The inclusion of an allergen avoidance arm in studies using animal models of allergic lung inflammation enables the assessment of biological resolution of the "disease state", and mimics clinical care, as patients diagnosed with allergic asthma are typically asked to avoid offending allergens. Previous studies in animal models show that allergen avoidance decreases cytokine abundance and immune cell number in the lungs after a course of repeated allergen challenge [108, 177]. As such, we employed an allergen avoidance arm to assess the reliability of using optical imaging to track changes in ProSense750 over a two week period. We also assessed the correlation of quantitative optical imaging with a gold standard measurement of lung inflammation: immune cell counting in lavage obtained from murine lungs.

Our data revealed a somewhat surprising temporal pattern, as thoracic ProSense750 radiance that was elevated by repeated HDM challenge was sustained at this level through 2-weeks of allergen avoidance. Indeed, though not statistically significant, there appeared to be a trend for increasing cathepsin-activated ProSense750 radiance in the thorax region two weeks after initiating allergen avoidance. This trend was in contrast to the decline we observed for total immune cell number in lung lavage, as well as that for individual immune cell types. The immune cell count data that we obtained is consistent with published studies; total cell count and differential cell count decreasing to near basal levels within two weeks [108, 177].

The data we have collected suggest that despite egress or turnover of recruited immune cells from the allergen-challenged lung, a residual elevated signature of cathepsin activity remains. There is increased abundance and diversity of cathepsin enzymes expressed in the lung tissue during an asthmatic response [174]. Indeed, cathepsin expression by structural cells such as airway epithelium, fibroblasts and airway smooth muscle cells is well documented and likely contributes to increased cathepsin expression and activity in asthma [50, 178, 179]. Though the scope of our studies did not include direct measurement of individual cathepsin subtypes in the lung and immune cells, our findings strongly suggest that future studies are needed to more precisely track the retention of cathepsin activity in the lung after allergen insult is ceased. To our knowledge, though prior studies have examined the induction of cathepsin expression and activity in asthma-like conditions [41, 42, 55, 56, 70, 109], our data is the first describing the longevity, and as such little mechanistic insight exists to account for this phenomenon.

During our allergen avoidance protocol we assessed the correlation of thoracic ProSense750 radiance with immune cell counts obtained from lung lavage. In individual mice, there was weak correlation of ProSense750 radiance with total immune cell number. The lack of correlation was also evident between ProSense750 radiance and individual immune cell number in lung lavage. This was somewhat surprising, but is reflective of the temporal pattern for sustained ProSense750 radiance that we observed during allergen avoidance. As described in the previous section, the lung may be somewhat unique in the capacity for resident cells for elevated expression and activation of cathepsins. Moreover, the lung is rich in alveolar macrophages that are also a source for cathepsins [180], however, these phagocytic cells are a principal driver for removing active and dying immune cells (ie efferocytosis) [181]. A limitation of our experimental design may be in our use of only the ProSense750 tracker. It relies on cathepsin

activation, but cathepsins are not expressed by a specific immune cell or structural cell subtype, thus our measurements reflect a broader spectrum of cell-associated activity. Future studies should employ cell specific inflammation markers, such as a cleavage-activated dye targeted by neutrophil elastase, a neutrophil specific marker [182]. Another caveat is that our experiments reveal that the biological process associated with suppression of inflammation during allergen avoidance unexpectedly includes sustained cathepsin activity. This appears to be supported by our observation that the correlation of ProSense750 radiance with immune cell counts in active inflammation post-allergen challenge was much stronger**,** as we observed that by binning cell counts based on their magnitude into three groups, and including allergen-naïve mice, there was correlation with immune cell number in allergen-challenged mice, including those subjected to allergen avoidance. The importance of our efforts to correlate immune number data with ProSense750 radiance was to assess technical feasibility of using ProSense750 radiance as an exclusive marker of inflammation over time in individual mice. Though in principle this remains an attractive approach, out data clearly show that for ProSense750, the biological processes that regulate activation of the dye are more complex that just immune cell influx, thus, caution is necessary in the interpretation of data using this dye as an index of inflammation in a traditional sense.

10.7 Simvastatin and Fluticasone treatment

Our findings using allergen avoidance suggest that cathepsin biology can be uncoupled from inflammatory cell resolution, thus optical imaging with ProSense750 offers an opportunity to determine whether similar unique pathobiological process may exist using pharmacotherapeutic options. Our studies confirm that ProSense750 lung radiance is

significantly greater in HDM-challenged mice compared to allergen-naïve mice, thus we next aimed to assess whether optical imaging was sufficient to detect anti-inflammatory effects of existing and potential asthma therapeutics.

Fluticasone propionate is an established first line asthma therapy to control and suppress lung inflammation [158]. Work in our lab has also revealed that inhaled simvastatin has anti-inflammatory effects in HDM-challenged mice however the precise mechanism for this effect is not known [158, 183-185] This work included studies by other members of our group also reveal that inhaled simvastatin exhibits a dose-dependent effect on lung immune cell number in HDM-challenged mice, thus provides a platform for assessing incremental changes in lung inflammation using ProSense750 thoracic imaging. These findings are consistent with others in the field that show statins can mitigate allergic lung inflammation in small animal models of asthma [42, 184]. The studies performed herein with intra nasally instilled simvastatin demonstrate that ProSense750 thoracic radiance is blunted in a dose-dependent manner. In contrast to our results using allergen avoidance, loss of ProSense750 radiance and lung lavage immune cell number correlated well. Conversely, my studies using intranasal instilled fluticasone propionate revealed a relative increase in ProSense750 lung radiance in both allergen-naïve and HDM-challenged mice. This occurred despite significant inhibition of immune cell infiltration to the lungs by fluticasone propionate treatment, revealing a similar pattern to that we observed during allergen avoidance.

The underpinnings for the disparities we observe in lung immune cell number and lung ProSense750 radiance during simvastatin or fluticasone propionate therapy may be rooted in disparate mechanism of action of each therapeutic option. Simvastatin inhibits the proximal enzyme of the mevalonate cascade, HMG-CoA, and in-so-doing depletes cells of sterol

precursors (isoprenoids), which are used as lipid anchors that are required for activation of a number of critical signaling proteins, including those of the Ras Super Family [186]. This effect is associated with blunting of trophic and secretory activity of immune and structural cells, for example a significant inhibition of interleukin-6 biosynthesis, a known mediator of the allergic response [15, 24, 45]. Indeed simvastatin prevents the expression of various cytokines, including those that initiate and coordinate the inflammatory response [17, 28, 187]. Steroids bind receptors that act as transcription factors that can induce or inhibit expression of genes that lead to blunted inflammation. Fluticasone propionate thus inhibits the formation of various interleukins and eosinophil-specific compounds in murine models of allergic asthma [187]. The degree to which the effects of simvastatin or fluticasone propionate directly affect regulatory mechanisms that control cathepsin expression and release are not known, however our finding suggest these differ fundamentally.

Cathepsins have remained relatively overlooked as a protease during inflammation studies. They are found primarily in the lysosome of the cell and can be released to degrade the surrounding matrix during inflammation and the wound repair response, with cathepsin C, S, and D being are primarily responsible for activity in inflammatory sites [41]. A number of *in vivo* studies reveal that cathepsin activation is associated with various lung complications such as emphysemaytous process in IFNγ transgenic mice [188]. Cathepsins are also associated with processing and activation of Toll-like receptors (TLR) that are a central control mechanism for immunity and inflammation [18]. This relatively poorly understood mechanism could be a critical determinant of the immune response in murine lungs challenged with HDM, as the dust mite allergen preparation includes TLR ligands such as the lipopolysaccharide complex, endotoxin (LPS). The sources of cathepsins in the lung in response to HDM challenge are not

completely elucidated, however based on our optical imaging evidence using ProSense750, in addition to immune cells such as eosinophils, neutrophils and macrophages, as has been reported, structural cells of the lungs are likely a significant source of cathepsins. This could explain the sustained cathepsin activity that we observe in HDM-challenged mice during allergen avoidance, or steroid therapy. As for the latter, there is evidence that inhaled steroids to injure or stress airway epithelial cells [171], thus we speculate that this may underpin the excess ProSense750 radiance that we detect in allergen-naïve mice and in HDM-challenged mice treated with fluticasone propionate. Our data also bring to light a potential role for sustained cathepsin activity as a biological mechanism associated with structural changes in the airways and lung during chronic asthma. The proteolytic nature of cathepsins positions them as modulators of the extracellular microenvironment and tissue remodeling.

10.9 Autophagy and chloroquine

Autophagy has become of interest in recent years as a mechanism regulating asthma pathogenesis and pathophysiology, however whether it is a pro-pathologic or inhibitory mechanism has not been resolved. Nonetheless, there are a number of reports that link the presence of autophagy in lung structural cells in biopsies from asthmatic subjects and has been hypothesized to influence asthmatic markers such as Th2 cytokines associated with the inflammatory response [25, 47, 189]. Due to this uncertainty in the field, the autophagy studies presented in this thesis was performed in two steps. First, using cultured human airway smooth muscle cells to determine whether asthma-associated inflammatory mediators induce an autophagy response. Second, using optical imaging with ProSense750 and immune cell counting

in lung lavage, determine the effect of an anti-autophagy agent, chloroquine, on HDM challenge-induced allergic lung inflammation in mice.

As a gold standard marker for autophagy induction, we tracked abundance of the autophagosome marker, LC3-II, in airway smooth muscle cells after exposure to IFNγ/THFα/IL-1β. We demonstrate that these cytokines are sufficient to induce autophagy in lung cells. Our findings are consistent with prior reports that examined LC3-II expression induced by individual cytokines in various lung cell types, including epithelial and smooth muscle [82, 83]. Collectively, these data confirm an association of autophagy in lung cells and asthma pathobiology, thus supporting rationale for our next set of studies to assess the impact of chloroquine therapy on lung inflammation in HDM-challenged mice.

Chloroquine was administered systemically to mice during HDM challenge, thus our experiment assesses whether this treatment prevents induction of asthma-like pathophysiology. Chloroquine prevents lysosomal fusion as well as preventing endosomal acidification, thus prevents completion of the autophagy cascade [190]. Notably, intracellular cathepsins are primarily located in the lysosome, thus chloroquine holds interesting promise in regulating cathepsin activation and release. However, optical imaging did not demonstrate any impact of chloroquine treatment in thoracic ProSense750 radiance in HDM-challenged or allergen-naïve mice. In contrast, chloroquine therapy did significantly reduce HDM challenge-induced accumulation of immune cells in the lung. Based on our *in vitro* findings that inflammatory mediators induce autophagy, the anti-inflammatory effects of chloroquine may be associated with suppression of autophagy induction by inflammatory mediators released in response to HDM challenge. This effect is corroborated by other studies looking at autophagy's effects on inflammatory markers in other disease states [19, 27, 45, 73, 76, 92, 110]. The reasons for a lack-

of-change in the ProSense750 thoracic radiance are not obvious, but it would appear that inhibition of lysosome fusion is not sufficient to prevent cathepsin release and activation.

10.10 Conclusions and Future Directions

This thesis presents the first assessment of the utility of optical fluorescent imaging as a way to measure the inflammatory response associated with allergic asthma in *in vivo* models. Non-invasive medical imaging provides a unique opportunity for repeated measurement of pathophysiologically relevant processes over the course of disease genesis and response to treatment in animal models. Lung imaging is complicated by the lack of tissue density and high airspace volume, thus optical imaging that using fluorescent tracer dyes hold particular promise to track biological processes. Our studies reveal that fluorescent optical imaging with an enzyme-activated dye can be used to measure differences in lung inflammation between HDM-challenged and allergen-naïve mice. We show here that using a cathepsin-activated tracer, ProSesnse750, fluorescence optical imaging enables measurement of a unique feature of inflammation. Importantly, our data demonstrate that the correlation of ProSense750 radiance is not a direct index of total immune cell influx to the lungs; rather we have uncovered a mechanism that can be independent of immune cell influx. A unique observation from our work is that cathepsin-capable activation of ProSesne750 is retained well after immune cells are cleared from the lung. These observations indicate that either resident tissue cells represent a significant source for cathepsin biosynthesis and/or that cathepsins released by immune cells as they turn over are retained and possess stable activity. The degree to which this may contribute to ongoing pathobiology or tissue repair is unclear, but the findings in this thesis have uncovered a novel key question for follow up studies. Interestingly we have demonstrated a disparate effect

of asthma therapies such as allergen avoidance, fluticasone propionate, and intranasal instilled simvastatin on sustained cathepsin-induced ProSense750 lung radiance. These observations suggest that cathepsin contributions to asthma pathophysiology, disease progression or disease control may underpin limitations to the success of asthma therapies. Overall, this thesis demonstrates that non-invasive optical imaging can provide complementary and deeper insight than more conventional methods that measure cell influx to quantify inflammation.

Our work identifies a number of new directions for future research. First, as ProSense750 radiance is an indirect index of cathepsin activity it does not reveal the identity of the specific cathepsin isoforms that contribute to inflammation or response to therapy. Our findings provide strong rationale for future studies that more directly examine cell-specific cathepsin expression and release, as well as the mechanisms that regulate activation and maintenance of cathepsin activity. Our results suggest that the tracer dye used for optical imaging is critical in demonstrating otherwise unappreciated mechanisms. This highlights an important opportunity as the repertoire of commercially available cleavage-activated dyes that are becoming available is broad and growing. Current dyes that should be investigated for their unique association with lung inflammation and lung tissue remodeling include those that track angiogenesis, neutrophil elastase activity, matrix metalloproteinase activity and apoptosis, for example. Such studies have significant potential to lead to new discoveries about molecular processes in asthma and lung inflammation. Finally, as we demonstrate that optical imaging is a relatively easy-to-use method for repeated screening of individual animals, our work suggests that this platform is well suited for, and should be used in preclinical studies for drug screening and to elucidate disease processes.

11. REFERENCES

1. Holgate, S.T. and R. Polosa, *Treatment strategies for allergy and asthma.* Nat Rev Immunol, 2008. **8**(3): p. 218-30.
2. Boulet, L.P., et al., *What is new since the last (1999) Canadian Asthma Consensus Guidelines?* Can Respir J, 2001. **8 Suppl A**: p. 5A-27A.
3. Bergeron, C., W. Al-Ramli, and Q. Hamid, *Remodeling in asthma.* Proc Am Thorac Soc, 2009. **6**(3): p. 301-5.
4. Grainge, C.L., et al., *Effect of bronchoconstriction on airway remodeling in asthma.* N Engl J Med, 2011. **364**(21): p. 2006-15.
5. Renauld, J.C., *New insights into the role of cytokines in asthma.* J Clin Pathol, 2001. **54**(8): p. 577-89.
6. Thomson, N.C. and M. Spears, *The influence of smoking on the treatment response in patients with asthma.* Curr Opin Allergy Clin Immunol, 2005. **5**(1): p. 57-63.
7. Rabe, K.F., et al., *Global strategy for the diagnosis, management, and prevention of chronic obstructive pulmonary disease: GOLD executive summary.* Am J Respir Crit Care Med, 2007. **176**(6): p. 532-55.
8. Pauwels, R.A., et al., *Global strategy for the diagnosis, management, and prevention of chronic obstructive pulmonary disease. NHLBI/WHO Global Initiative for Chronic Obstructive Lung Disease (GOLD) Workshop summary.* Am J Respir Crit Care Med, 2001. **163**(5): p. 1256-76.
9. Luize, A.P., et al., *Assessment of five different guideline indication criteria for spirometry, including modified GOLD criteria, in order to detect COPD: data from 5,315 subjects in the PLATINO study.* NPJ Prim Care Respir Med, 2014. **24**: p. 14075.
10. Bateman, E.D., et al., *Global strategy for asthma management and prevention: GINA executive summary.* Eur Respir J, 2008. **31**(1): p. 143-78.
11. Qaseem, A., et al., *Diagnosis and management of stable chronic obstructive pulmonary disease: a clinical practice guideline update from the American College of Physicians, American College of Chest Physicians, American Thoracic Society, and European Respiratory Society.* Ann Intern Med, 2011. **155**(3): p. 179-91.
12. Yu, M., et al., *Mast cells can promote the development of multiple features of chronic asthma in mice.* J Clin Invest, 2006. **116**(6): p. 1633-41.
13. Fahy, J.V., *Eosinophilic and neutrophilic inflammation in asthma: insights from clinical studies.* Proc Am Thorac Soc, 2009. **6**(3): p. 256-9.
14. Robinson, D.S., *The role of the mast cell in asthma: induction of airway hyperresponsiveness by interaction with smooth muscle?* J Allergy Clin Immunol, 2004. **114**(1): p. 58-65.
15. Ngoc, P.L., et al., *Cytokines, allergy, and asthma.* Curr Opin Allergy Clin Immunol, 2005. **5**(2): p. 161-6.
16. Rudmann, D.G., et al., *Modulation of allergic inflammation in mice deficient in TNF receptors.* Am J Physiol Lung Cell Mol Physiol, 2000. **279**(6): p. L1047-57.
17. Kumar, R.K., et al., *Interferon-gamma as a possible target in chronic asthma.* Inflamm Allergy Drug Targets, 2006. **5**(4): p. 253-6.
18. Homma, T., et al., *Involvement of TLR2 and EGFR Signaling in Epithelial Expression of Airway Remodeling Factors.* Am J Respir Cell Mol Biol, 2014.

19. Holgate, S.T., *The sentinel role of the airway epithelium in asthma pathogenesis.* Immunol Rev, 2011. **242**(1): p. 205-19.
20. Tliba, O., Y. Amrani, and R.A. Panettieri, Jr., *Is airway smooth muscle the "missing link" modulating airway inflammation in asthma?* Chest, 2008. **133**(1): p. 236-42.
21. Noble, P.B., et al., *Airway smooth muscle in asthma: Linking contraction and mechanotransduction to disease pathogenesis and remodelling.* Pulm Pharmacol Ther, 2014.
22. James, A.L., et al., *The relationship of reticular basement membrane thickness to airway wall remodeling in asthma.* Am J Respir Crit Care Med, 2002. **166**(12 Pt 1): p. 1590-5.
23. Knight, D., *Epithelium-fibroblast interactions in response to airway inflammation.* Immunol Cell Biol, 2001. **79**(2): p. 160-4.
24. Doherty, T. and D. Broide, *Cytokines and growth factors in airway remodeling in asthma.* Curr Opin Immunol, 2007. **19**(6): p. 676-80.
25. Mathias, C.B., *Natural killer cells in the development of asthma.* Curr Allergy Asthma Rep, 2015. **15**(2): p. 500.
26. Liu, Y.C., et al., *Macrophage polarization in inflammatory diseases.* Int J Biol Sci, 2014. **10**(5): p. 520-9.
27. Balhara, J. and A.S. Gounni, *The alveolar macrophages in asthma: a double-edged sword.* Mucosal Immunol, 2012. **5**(6): p. 605-9.
28. Romagnani, S., *Type 1 T helper and type 2 T helper cells: functions, regulation and role in protection and disease.* Int J Clin Lab Res, 1991. **21**(2): p. 152-8.
29. Gutcher, I. and B. Becher, *APC-derived cytokines and T cell polarization in autoimmune inflammation.* J Clin Invest, 2007. **117**(5): p. 1119-27.
30. Shedlock, D.J. and H. Shen, *Requirement for CD4 T cell help in generating functional CD8 T cell memory.* Science, 2003. **300**(5617): p. 337-9.
31. Steinman, R.M. and Z.A. Cohn, *Identification of a novel cell type in peripheral lymphoid organs of mice. I. Morphology, quantitation, tissue distribution.* J Exp Med, 1973. **137**(5): p. 1142-62.
32. Banchereau, J. and R.M. Steinman, *Dendritic cells and the control of immunity.* Nature, 1998. **392**(6673): p. 245-52.
33. Witko-Sarsat, V., et al., *Neutrophils: molecules, functions and pathophysiological aspects.* Lab Invest, 2000. **80**(5): p. 617-53.
34. Rothenberg, M.E. and S.P. Hogan, *The eosinophil.* Annu Rev Immunol, 2006. **24**: p. 147-74.
35. Hogan, S.P., et al., *Eosinophils: biological properties and role in health and disease.* Clin Exp Allergy, 2008. **38**(5): p. 709-50.
36. Mosser, D.M. and J.P. Edwards, *Exploring the full spectrum of macrophage activation.* Nat Rev Immunol, 2008. **8**(12): p. 958-69.
37. Gaurav, R. and D.K. Agrawal, *Clinical view on the importance of dendritic cells in asthma.* Expert Rev Clin Immunol, 2013. **9**(10): p. 899-919.
38. Hart, P.H., *Regulation of the inflammatory response in asthma by mast cell products.* Immunol Cell Biol, 2001. **79**(2): p. 149-53.
39. Palikhe, N.S., et al., *Association of three sets of high-affinity IgE receptor (FcepsilonR1) polymorphisms with aspirin-intolerant asthma.* Respir Med, 2008. **102**(8): p. 1132-9.
40. Dumez, M.E., et al., *Orchestration of an uncommon maturation cascade of the house dust mite protease allergen quartet.* Front Immunol, 2014. **5**: p. 138.

41. Faiz, A., et al., *The expression and activity of cathepsins D, H and K in asthmatic airways.* PLoS One, 2013. **8**(3): p. e57245.
42. Lalmanach, G., et al., *Cysteine cathepsins and cystatins: from ancillary tasks to prominent status in lung diseases.* Biol Chem, 2014.
43. Li, J., et al., *Interleukin-4 and interleukin-13 pathway genetics affect disease susceptibility, serum immunoglobulin E levels, and gene expression in asthma.* Ann Allergy Asthma Immunol, 2014. **113**(2): p. 173-179 e1.
44. Garcia, G., et al., *Anti-interleukin-5 therapy in severe asthma.* Eur Respir Rev, 2013. **22**(129): p. 251-7.
45. Farahani, R., et al., *Cytokines (interleukin-9, IL-17, IL-22, IL-25 and IL-33) and asthma.* Adv Biomed Res, 2014. **3**: p. 127.
46. Saatian, B., et al., *Interleukin-4 and interleukin-13 cause barrier dysfunction in human airway epithelial cells.* Tissue Barriers, 2013. **1**(2): p. e24333.
47. Georas, S.N. and F. Rezaee, *Epithelial barrier function: at the front line of asthma immunology and allergic airway inflammation.* J Allergy Clin Immunol, 2014. **134**(3): p. 509-20.
48. Sugita, M., et al., *Allergic bronchial asthma: airway inflammation and hyperresponsiveness.* Intern Med, 2003. **42**(8): p. 636-43.
49. Venkatasamy, R. and D. Spina, *Protease inhibitors in respiratory disease: focus on asthma and chronic obstructive pulmonary disease.* Expert Rev Clin Immunol, 2007. **3**(3): p. 365-81.
50. Chilosi, M., et al., *Cathepsin-k expression in pulmonary lymphangioleiomyomatosis.* Mod Pathol, 2009. **22**(2): p. 161-6.
51. Fonovic, M. and B. Turk, *Cysteine cathepsins and extracellular matrix degradation.* Biochim Biophys Acta, 2014. **1840**(8): p. 2560-70.
52. Asagiri, M., et al., *Cathepsin K-dependent toll-like receptor 9 signaling revealed in experimental arthritis.* Science, 2008. **319**(5863): p. 624-7.
53. Turk, V., et al., *Cysteine cathepsins: from structure, function and regulation to new frontiers.* Biochim Biophys Acta, 2012. **1824**(1): p. 68-88.
54. Guncar, G., et al., *Crystal structure of MHC class II-associated p41 Ii fragment bound to cathepsin L reveals the structural basis for differentiation between cathepsins L and S.* EMBO J, 1999. **18**(4): p. 793-803.
55. Deschamps, K., et al., *Genetic and pharmacological evaluation of cathepsin s in a mouse model of asthma.* Am J Respir Cell Mol Biol, 2011. **45**(1): p. 81-7.
56. Cimerman, N., et al., *Serum concentration and circadian profiles of cathepsins B, H and L, and their inhibitors, stefins A and B, in asthma.* Clin Chim Acta, 2001. **310**(2): p. 113-22.
57. Bergmann, M. and J.S. Fruton, *Regarding the General Nature of Catheptic Enzymes.* Science, 1936. **84**(2169): p. 89-90.
58. Takiguchi, K., et al., *Structural and functional study of K453E mutant protective protein/cathepsin A causing the late infantile form of galactosialidosis.* J Hum Genet, 2000. **45**(4): p. 200-6.
59. Kindy, M.S., et al., *Deletion of the cathepsin B gene improves memory deficits in a transgenic ALZHeimer's disease mouse model expressing AbetaPP containing the wild-type beta-secretase site sequence.* J Alzheimers Dis, 2012. **29**(4): p. 827-40.

60. Wani, A.A., et al., *Description of two new cathepsin C gene mutations in patients with Papillon-Lefevre syndrome.* J Periodontol, 2006. **77**(2): p. 233-7.
61. Meade, J.L., et al., *A family with Papillon-Lefevre syndrome reveals a requirement for cathepsin C in granzyme B activation and NK cell cytolytic activity.* Blood, 2006. **107**(9): p. 3665-8.
62. Ozkayar, N., et al., *Relation between serum cathepsin D levels and endothelial dysfunction in patients with chronic kidney disease.* Nefrologia, 2015. **35**(1): p. 72-9.
63. Zaidi, N. and H. Kalbacher, *Cathepsin E: a mini review.* Biochem Biophys Res Commun, 2008. **367**(3): p. 517-22.
64. Armao, D., et al., *Neutral proteases and disruption of the blood-brain barrier in rat.* Brain Res, 1997. **767**(2): p. 259-64.
65. Thorsen, S.U., et al., *Polymorphisms in the CTSH gene may influence the progression of diabetic retinopathy: a candidate-gene study in the Danish Cohort of Pediatric Diabetes 1987 (DCPD1987).* Graefes Arch Clin Exp Ophthalmol, 2015. **253**(11): p. 1959-65.
66. Drake, M.T., et al., *Cathepsin K Inhibitors for Osteoporosis: Biology, Potential Clinical Utility, and Lessons Learned.* Endocr Rev, 2017. **38**(4): p. 325-350.
67. Barrett, A.J. and H. Kirschke, *Cathepsin B, Cathepsin H, and cathepsin L.* Methods Enzymol, 1981. **80 Pt C**: p. 535-61.
68. Xu, J., et al., *Inhibition of cathepsin S produces neuroprotective effects after traumatic brain injury in mice.* Mediators Inflamm, 2013. **2013**: p. 187873.
69. Huang, K., et al., *Exogenous cathepsin V protein protects human cardiomyocytes HCM from angiotensin -Induced hypertrophy.* Int J Biochem Cell Biol, 2017. **89**: p. 6-15.
70. Fajardo, I., et al., *Increased levels of hypoxia-sensitive proteins in allergic airway inflammation.* Am J Respir Crit Care Med, 2004. **170**(5): p. 477-84.
71. Lewis, C.C., et al., *Disease-specific gene expression profiling in multiple models of lung disease.* Am J Respir Crit Care Med, 2008. **177**(4): p. 376-87.
72. Hirakawa, H., et al., *Cathepsin S deficiency confers protection from neonatal hyperoxia-induced lung injury.* Am J Respir Crit Care Med, 2007. **176**(8): p. 778-85.
73. Lambrecht, B.N. and H. Hammad, *The immunology of asthma.* Nat Immunol, 2014. **16**(1): p. 45-56.
74. Olson, O.C. and J.A. Joyce, *Cysteine cathepsin proteases: regulators of cancer progression and therapeutic response.* Nat Rev Cancer, 2015. **15**(12): p. 712-29.
75. Lin, N.Y., et al., *Autophagy regulates TNFalpha-mediated joint destruction in experimental arthritis.* Ann Rheum Dis, 2013. **72**(5): p. 761-8.
76. Jyothula, S.S. and N.T. Eissa, *Autophagy and role in asthma.* Curr Opin Pulm Med, 2013. **19**(1): p. 30-5.
77. Levine, B. and D.J. Klionsky, *Development by self-digestion: molecular mechanisms and biological functions of autophagy.* Dev Cell, 2004. **6**(4): p. 463-77.
78. Liu, Y. and B. Levine, *Autosis and autophagic cell death: the dark side of autophagy.* Cell Death Differ, 2014.
79. Peric, A. and W. Annaert, *Early etiology of Alzheimer's disease: tipping the balance toward autophagy or endosomal dysfunction?* Acta Neuropathol, 2015.
80. Vindis, C., *Autophagy: an emerging therapeutic target in vascular diseases.* Br J Pharmacol, 2014.
81. Xiao, M.J. and L.G. Li, *[Research progress on autophagy regulating excessive inflammation].* Sheng Li Xue Bao, 2014. **66**(6): p. 739-45.

82. Ghavami, S., et al., *Geranylgeranyl transferase 1 modulates autophagy and apoptosis in human airway smooth muscle.* Am J Physiol Lung Cell Mol Physiol, 2012. **302**(4): p. L420-8.
83. Juarez, E., et al., *Nucleotide-oligomerizing domain-1 (NOD1) receptor activation induces pro-inflammatory responses and autophagy in human alveolar macrophages.* BMC Pulm Med, 2014. **14**: p. 152.
84. Stamatiou, R., et al., *Azithromycin has an antiproliferative and autophagic effect on airway smooth muscle cells.* Eur Respir J, 2009. **34**(3): p. 721-30.
85. O'Byrne, P.M., G.M. Gauvreau, and J.D. Brannan, *Provoked models of asthma: what have we learnt?* Clin Exp Allergy, 2009. **39**(2): p. 181-92.
86. Finkelman, F.D. and M. Wills-Karp, *Usefulness and optimization of mouse models of allergic airway disease.* J Allergy Clin Immunol, 2008. **121**(3): p. 603-6.
87. Phalen, R.F., M.J. Oldham, and R.K. Wolff, *The relevance of animal models for aerosol studies.* J Aerosol Med Pulm Drug Deliv, 2008. **21**(1): p. 113-24.
88. Zosky, G.R. and P.D. Sly, *Animal models of asthma.* Clin Exp Allergy, 2007. **37**(7): p. 973-88.
89. Costa Carvalho, J.L., et al., *The chemokines secretion and the oxidative stress are targets of low-level laser therapy in allergic lung inflammation.* J Biophotonics, 2016.
90. Shi, J.P., et al., *P2Y6 contributes to ovalbumin-induced allergic asthma by enhancing mast cell function in mice.* Oncotarget, 2016.
91. Gold, M., D. Marsolais, and M.R. Blanchet, *Mouse models of allergic asthma.* Methods Mol Biol, 2015. **1220**: p. 503-19.
92. Fan, M. and S. Jamal Mustafa, *Role of adenosine in airway inflammation in an allergic mouse model of asthma.* Int Immunopharmacol, 2006. **6**(1): p. 36-45.
93. Mehlhop, P.D., et al., *Allergen-induced bronchial hyperreactivity and eosinophilic inflammation occur in the absence of IgE in a mouse model of asthma.* Proc Natl Acad Sci U S A, 1997. **94**(4): p. 1344-9.
94. Lundy, S.K., A.A. Berlin, and N.W. Lukacs, *Interleukin-12-independent down-modulation of cockroach antigen-induced asthma in mice by intranasal exposure to bacterial lipopolysaccharide.* Am J Pathol, 2003. **163**(5): p. 1961-8.
95. Zosky, G.R., et al., *The pattern of methacholine responsiveness in mice is dependent on antigen challenge dose.* Respir Res, 2004. **5**: p. 15.
96. Johnson, J.R., et al., *Continuous exposure to house dust mite elicits chronic airway inflammation and structural remodeling.* Am J Respir Crit Care Med, 2004. **169**(3): p. 378-85.
97. Piyadasa, H., et al., *Biosignature for airway inflammation in a house dust mite-challenged murine model of allergic asthma.* Biol Open, 2016. **5**(2): p. 112-21.
98. Shima, K., et al., *Effects of sublingual immunotherapy in a murine asthma model sensitized by intranasal administration of house dust mite extracts.* Allergol Int, 2016.
99. Tashiro, H., et al., *Interleukin-33 from Monocytes Recruited to the Lung Contributes to House Dust Mite-Induced Airway Inflammation in a Mouse Model.* PLoS One, 2016. **11**(6): p. e0157571.
100. McGovern, T.K., et al., *Neutrophilic oxidative stress mediates organic dust-induced pulmonary inflammation and airway hyperresponsiveness.* Am J Physiol Lung Cell Mol Physiol, 2016. **310**(2): p. L155-65.

101. Edukulla, R., et al., *Intratracheal myriocin enhances allergen-induced Th2 inflammation and airway hyper-responsiveness.* Immun Inflamm Dis, 2016. **4**(3): p. 248-62.
102. Ryu, M.H., et al., *Chronic exposure to perfluorinated compounds: Impact on airway hyperresponsiveness and inflammation.* Am J Physiol Lung Cell Mol Physiol, 2014. **307**(10): p. L765-74.
103. Braun, A., et al., *Role of nerve growth factor in a mouse model of allergic airway inflammation and asthma.* Eur J Immunol, 1998. **28**(10): p. 3240-51.
104. Zhang, D.H., et al., *Inhibition of allergic inflammation in a murine model of asthma by expression of a dominant-negative mutant of GATA-3.* Immunity, 1999. **11**(4): p. 473-82.
105. Malm-Erjefalt, M., C.G. Persson, and J.S. Erjefalt, *Degranulation status of airway tissue eosinophils in mouse models of allergic airway inflammation.* Am J Respir Cell Mol Biol, 2001. **24**(3): p. 352-9.
106. Kumar, R.K. and P.S. Foster, *Modeling allergic asthma in mice: pitfalls and opportunities.* Am J Respir Cell Mol Biol, 2002. **27**(3): p. 267-72.
107. Erjefalt, J.S. and C.G. Persson, *New aspects of degranulation and fates of airway mucosal eosinophils.* Am J Respir Crit Care Med, 2000. **161**(6): p. 2074-85.
108. Cho, J.Y., et al., *Combination of corticosteroid therapy and allergen avoidance reverses allergen-induced airway remodeling in mice.* J Allergy Clin Immunol, 2005. **116**(5): p. 1116-22.
109. Korideck, H. and J.D. Peterson, *Noninvasive quantitative tomography of the therapeutic response to dexamethasone in ovalbumin-induced murine asthma.* J Pharmacol Exp Ther, 2009. **329**(3): p. 882-9.
110. Boyce, J.A. and K.F. Austen, *No audible wheezing: nuggets and conundrums from mouse asthma models.* J Exp Med, 2005. **201**(12): p. 1869-73.
111. Fine, E.J., et al., *Small-animal research imaging devices.* Semin Nucl Med, 2014. **44**(1): p. 57-65.
112. Thornton, E.E., M.F. Krummel, and M.R. Looney, *Live imaging of the lung.* Curr Protoc Cytom, 2012. **Chapter 12**: p. Unit12 28.
113. Harby, K., *MR microscopy: a new window to the lungs.* Mol Med Today, 1996. **2**(4): p. 139.
114. Moller, H.E., et al., *MRI of the lungs using hyperpolarized noble gases.* Magn Reson Med, 2002. **47**(6): p. 1029-51.
115. Mitzner, W., R. Brown, and W. Lee, *In vivo measurement of lung volumes in mice.* Physiol Genomics, 2001. **4**(3): p. 215-21.
116. Cutillo, A.G., et al., *Characterization of bleomycin lung injury by nuclear magnetic resonance: correlation between NMR relaxation times and lung water and collagen content.* Magn Reson Med, 2002. **47**(2): p. 246-56.
117. Beckmann, N., et al., *MRI of lung parenchyma in rats and mice using a gradient-echo sequence.* NMR Biomed, 2001. **14**(5): p. 297-306.
118. Hedlund, L.W. and G.A. Johnson, *Mechanical ventilation for imaging the small animal lung.* ILAR J, 2002. **43**(3): p. 159-74.
119. Flors, L., et al., *New insights into lung diseases using hyperpolarized gas MRI.* Radiologia, 2015. **57**(4): p. 303-13.
120. Schuster, D.P., *Positron emission tomography: theory and its application to the study of lung disease.* Am Rev Respir Dis, 1989. **139**(3): p. 818-40.

121. Schuster, D.P., *The evaluation of lung function with PET.* Semin Nucl Med, 1998. **28**(4): p. 341-51.
122. Hatori, A., et al., *PET imaging of lung inflammation with [18F]FEDAC, a radioligand for translocator protein (18 kDa).* PLoS One, 2012. **7**(9): p. e45065.
123. Chatziioannou, A.F., *Molecular imaging of small animals with dedicated PET tomographs.* Eur J Nucl Med Mol Imaging, 2002. **29**(1): p. 98-114.
124. Simon, B.A., *Non-invasive imaging of regional lung function using x-ray computed tomography.* J Clin Monit Comput, 2000. **16**(5-6): p. 433-42.
125. Paulus, M.J., et al., *High resolution X-ray computed tomography: an emerging tool for small animal cancer research.* Neoplasia, 2000. **2**(1-2): p. 62-70.
126. Bayat, S., et al., *Imaging of lung function using synchrotron radiation computed tomography: what's new?* Eur J Radiol, 2008. **68**(3 Suppl): p. S78-83.
127. Massoud, T.F. and S.S. Gambhir, *Molecular imaging in living subjects: seeing fundamental biological processes in a new light.* Genes Dev, 2003. **17**(5): p. 545-80.
128. Weissleder, R. and U. Mahmood, *Molecular imaging.* Radiology, 2001. **219**(2): p. 316-33.
129. Vooijs, M., et al., *Noninvasive imaging of spontaneous retinoblastoma pathway-dependent tumors in mice.* Cancer Res, 2002. **62**(6): p. 1862-7.
130. Edinger, M., et al., *Revealing lymphoma growth and the efficacy of immune cell therapies using in vivo bioluminescence imaging.* Blood, 2003. **101**(2): p. 640-8.
131. Hillman, E.M., et al., *In vivo optical imaging and dynamic contrast methods for biomedical research.* Philos Trans A Math Phys Eng Sci, 2011. **369**(1955): p. 4620-43.
132. Yang, X., et al., *Combined system of fluorescence diffuse optical tomography and microcomputed tomography for small animal imaging.* Rev Sci Instrum, 2010. **81**(5): p. 054304.
133. Pradhan, A., et al., *Steady state and time-resolved fluorescence properties of metastatic and non-metastatic malignant cells from different species.* J Photochem Photobiol B, 1995. **31**(3): p. 101-12.
134. Akers, W., et al., *In vivo resolution of multiexponential decays of multiple near-infrared molecular probes by fluorescence lifetime-gated whole-body time-resolved diffuse optical imaging.* Mol Imaging, 2007. **6**(4): p. 237-46.
135. Zhang, X., et al., *Near-infrared molecular probes for in vivo imaging.* Curr Protoc Cytom, 2012. **Chapter 12**: p. Unit12 27.
136. Pope, I., et al., *Coherent anti-Stokes Raman scattering microscopy of single nanodiamonds.* Nat Nanotechnol, 2014. **9**(11): p. 940-6.
137. Kawata, Y., Y. Nawa, and W. Inami, *High resolution fluorescent bio-imaging with electron beam excitation.* Microscopy (Oxf), 2014. **63 Suppl 1**: p. i16.
138. Soendergaard, M., J.R. Newton-Northup, and S.L. Deutscher, *In Vitro High-Throughput Phage Display Selection of Ovarian Cancer Avid Phage Clones for Near-Infrared Optical Imaging.* Comb Chem High Throughput Screen, 2014.
139. Puaux, A.L., et al., *A comparison of imaging techniques to monitor tumor growth and cancer progression in living animals.* Int J Mol Imaging, 2011. **2011**: p. 321538.
140. Zelmer, A. and T.H. Ward, *Noninvasive fluorescence imaging of small animals.* J Microsc, 2013. **252**(1): p. 8-15.
141. Looney, M.R. and J. Bhattacharya, *Live imaging of the lung.* Annu Rev Physiol, 2014. **76**: p. 431-45.

142. Balaban, R.S. and V.A. Hampshire, *Challenges in small animal noninvasive imaging.* ILAR J, 2001. **42**(3): p. 248-62.
143. Hong, G., et al., *Multifunctional in vivo vascular imaging using near-infrared II fluorescence.* Nat Med, 2012. **18**(12): p. 1841-6.
144. Welsher, K., S.P. Sherlock, and H. Dai, *Deep-tissue anatomical imaging of mice using carbon nanotube fluorophores in the second near-infrared window.* Proc Natl Acad Sci U S A, 2011. **108**(22): p. 8943-8.
145. Arnold, K.E., I.P. Owens, and N.J. Marshall, *Fluorescent signaling in parrots.* Science, 2002. **295**(5552): p. 92.
146. Roth, M.S., et al., *Green fluorescent protein regulation in the coral Acropora yongei during photoacclimation.* J Exp Biol, 2010. **213**(Pt 21): p. 3644-55.
147. Acuna, A.U., et al., *Structure and formation of the fluorescent compound of Lignum nephriticum.* Org Lett, 2009. **11**(14): p. 3020-3.
148. Bernard Valeur, M.N.B.-S., *Brief History of Fluorescence and Phosphorescence before the Emergence of Quantum Theory.* Journal of Chemical Education, 2011. **88**(6): p. 7.
149. Monici, M., *Cell and tissue autofluorescence research and diagnostic applications.* Biotechnol Annu Rev, 2005. **11**: p. 227-56.
150. Ding, S., et al., *Comparison of multiple enzyme activatable near-infrared fluorescent molecular probes for detection and quantification of inflammation in murine colitis models.* Inflamm Bowel Dis, 2014. **20**(2): p. 363-77.
151. Onda, N., et al., *In vivo imaging of tissue-remodeling activity involving infiltration of macrophages by a systemically administered protease-activatable probe in colon cancer tissues.* Transl Oncol, 2013. **6**(6): p. 628-37.
152. Hilderbrand, S.A. and R. Weissleder, *Near-infrared fluorescence: application to in vivo molecular imaging.* Curr Opin Chem Biol, 2010. **14**(1): p. 71-9.
153. Fernandez-Suarez, M. and A.Y. Ting, *Fluorescent probes for super-resolution imaging in living cells.* Nat Rev Mol Cell Biol, 2008. **9**(12): p. 929-43.
154. Cortez-Retamozo, V., et al., *Real-time assessment of inflammation and treatment response in a mouse model of allergic airway inflammation.* J Clin Invest, 2008. **118**(12): p. 4058-66.
155. Schols, R.M., N.J. Connell, and L.P. Stassen, *Near-Infrared Fluorescence Imaging for Real-Time Intraoperative Anatomical Guidance in Minimally Invasive Surgery: A Systematic Review of the Literature.* World J Surg, 2014.
156. Lin, C.C., et al., *The effect of serine protease inhibitors on airway inflammation in a chronic allergen-induced asthma mouse model.* Mediators Inflamm, 2014. **2014**: p. 879326.
157. Houari Korideck, J.D.P., *Noninvasive, In Vivo Quantitation of Asthma Severity using Fluorescence Molecular Tomography.* Nature Methods, 2008. **8**(5).
158. Bews, H.J., et al., *Simultaneous quantification of simvastatin and simvastatin hydroxy acid in blood serum at physiological pH by ultrahigh performance liquid chromatography-tandem mass spectrometry (UHPLC/MS/MS).* J Chromatogr B Analyt Technol Biomed Life Sci, 2014. **947-948**: p. 145-50.
159. Januskevicius, A., et al., *Suppression of Eosinophil Integrins Prevents Remodeling of Airway Smooth Muscle in Asthma.* Front Physiol, 2016. **7**: p. 680.

160. Koopmans, T., et al., *Selective targeting of CREB-binding protein/beta-catenin inhibits growth of and extracellular matrix remodelling by airway smooth muscle.* Br J Pharmacol, 2016. **173**(23): p. 3327-3341.
161. Anaparti, V., et al., *Tumor necrosis factor regulates NMDA receptor-mediated airway smooth muscle contractile function and airway responsiveness.* Am J Physiol Lung Cell Mol Physiol, 2016. **311**(2): p. L467-80.
162. Sotelo, J., E. Briceno, and M.A. Lopez-Gonzalez, *Adding chloroquine to conventional treatment for glioblastoma multiforme: a randomized, double-blind, placebo-controlled trial.* Ann Intern Med, 2006. **144**(5): p. 337-43.
163. Savarino, A., et al., *Risks and benefits of chloroquine use in anticancer strategies.* Lancet Oncol, 2006. **7**(10): p. 792-3.
164. Siontorou, C.G. and F.A. Batzias, *Innovation in biotechnology: moving from academic research to product development--the case of biosensors.* Crit Rev Biotechnol, 2010. **30**(2): p. 79-98.
165. Kennedy, D., *Government policies and the cost of doing research.* Science, 1985. **227**(4686): p. 480-4.
166. Galderisi, M., et al., *The multi-modality cardiac imaging approach to the Athlete's heart: an expert consensus of the European Association of Cardiovascular Imaging.* Eur Heart J Cardiovasc Imaging, 2015.
167. Lin, J.B., et al., *Imaging of Small Animal Peripheral Artery Disease Models: Recent Advancements and Translational Potential.* Int J Mol Sci, 2015. **16**(5): p. 11131-11177.
168. Tansi, F.L., et al., *Fluorescence-quenching of a liposomal-encapsulated near-infrared fluorophore as a tool for in vivo optical imaging.* J Vis Exp, 2015(95): p. e52136.
169. Troy, T., et al., *Quantitative comparison of the sensitivity of detection of fluorescent and bioluminescent reporters in animal models.* Mol Imaging, 2004. **3**(1): p. 9-23.
170. Cool, S.K., et al., *Comparison of in vivo optical systems for bioluminescence and fluorescence imaging.* J Fluoresc, 2013. **23**(5): p. 909-20.
171. Buhling, F., et al., *Cathepsin K--a marker of macrophage differentiation?* J Pathol, 2001. **195**(3): p. 375-82.
172. Lutgens, E., et al., *Disruption of the cathepsin K gene reduces atherosclerosis progression and induces plaque fibrosis but accelerates macrophage foam cell formation.* Circulation, 2006. **113**(1): p. 98-107.
173. Nomura, T. and N. Katunuma, *Involvement of cathepsins in the invasion, metastasis and proliferation of cancer cells.* J Med Invest, 2005. **52**(1-2): p. 1-9.
174. Oltmanns, U., et al., *Induction of human airway smooth muscle apoptosis by neutrophils and neutrophil elastase.* Am J Respir Cell Mol Biol, 2005. **32**(4): p. 334-41.
175. Salminen-Mankonen, H.J., J. Morko, and E. Vuorio, *Role of cathepsin K in normal joints and in the development of arthritis.* Curr Drug Targets, 2007. **8**(2): p. 315-23.
176. Song, C., et al., *IL-17-producing alveolar macrophages mediate allergic lung inflammation related to asthma.* J Immunol, 2008. **181**(9): p. 6117-24.
177. Johnson, J.R., et al., *Combined budesonide/formoterol therapy in conjunction with allergen avoidance ameliorates house dust mite-induced airway remodeling and dysfunction.* Am J Physiol Lung Cell Mol Physiol, 2008. **295**(5): p. L780-8.
178. Coyle, A.J., et al., *Role of cationic proteins in the airway. Hyperresponsiveness due to airway inflammation.* Am J Respir Crit Care Med, 1994. **150**(5 Pt 2): p. S63-71.

179. Gao, S., et al., *The role and mechanism of cathepsin G in dermatomyositis.* Biomed Pharmacother, 2017. **94**: p. 697-704.
180. Lesser, M., et al., *Cathepsin B and D activity in alveolar macrophages from rats with pulmonary granulomatous inflammation or acute lung injury.* Agents Actions, 1989. **28**(3-4): p. 264-71.
181. Belchamber, K.B.R. and L.E. Donnelly, *Macrophage Dysfunction in Respiratory Disease.* Results Probl Cell Differ, 2017. **62**: p. 299-313.
182. Glinzer, A., et al., *Targeting Elastase for Molecular Imaging of Early Atherosclerotic Lesions.* Arterioscler Thromb Vasc Biol, 2017. **37**(3): p. 525-533.
183. Tulbah, A.S., et al., *Inhaled simvastatin nanoparticles for inflammatory lung disease.* Nanomedicine (Lond), 2017. **12**(20): p. 2471-2485.
184. Gu, W., et al., *Simvastatin alleviates airway inflammation and remodelling through up-regulation of autophagy in mouse models of asthma.* Respirology, 2017. **22**(3): p. 533-541.
185. Schaafsma, D., et al., *Simvastatin inhibits TGFbeta1-induced fibronectin in human airway fibroblasts.* Respir Res, 2011. **12**: p. 113.
186. Ghittoni, R., et al., *Simvastatin inhibits the MHC class II pathway of antigen presentation by impairing Ras superfamily GTPases.* Eur J Immunol, 2006. **36**(11): p. 2885-93.
187. Gao, J. and R.A. Pleasants, *Role of the fixed combination of fluticasone and salmeterol in adult Chinese patients with asthma and COPD.* Int J Chron Obstruct Pulmon Dis, 2015. **10**: p. 775-789.
188. Ishii, T., et al., *IFN Regulatory Factor 3 Potentiates Emphysematous Aggravation by Lipopolysaccharide.* J Immunol, 2017. **198**(9): p. 3637-3649.
189. Bice, D.E., J. Seagrave, and F.H. Green, *Animal models of asthma: potential usefulness for studying health effects of inhaled particles.* Inhal Toxicol, 2000. **12**(9): p. 829-62.
190. Chen, P.M., Z.J. Gombart, and J.W. Chen, *Chloroquine treatment of ARPE-19 cells leads to lysosome dilation and intracellular lipid accumulation: possible implications of lysosomal dysfunction in macular degeneration.* Cell Biosci, 2011. **1**(1): p. 10.